Nuclear Instruments and Methods in Physics Research A 1070 (2025) 170031

Contents lists available at ScienceDirect

Nuclear Inst. and Methods in Physics Research, A

journal homepage: www.elsevier.com/locate/nima

Full Length Article

CETASim: A numerical tool for beam collective effect study in storage rings☆

Chao Li *, Yong-Chul Chae

Deutsches Elektronen Synchrotron, Notkestrasse 85, 22607 Hamburg, Germany

ARTICLE INFO

Keywords:
Electron storage rings
Beam collective effect
Impedance
Wakefield
CETASim

ABSTRACT

We developed a 6D multi-particle tracking program CETASim in C++ to simulate intensity-dependent effects in electron storage rings. The program can simulate the beam collective effects due to short-range/long-range wakefields for single/coupled-bunch instability studies. It also features the simulation of interactions among charged ions and the trains of electron bunches, including both fast ion and ion trapping effects. The bunch-by-bunch feedback is also included so that the user can simulate the damping of the unstable motion when its growth rate is faster than the radiation damping rate. The particle dynamics is based on the transfer maps from sector to sector, including the nonlinear effects of amplitude-dependent tune shift, high-order chromaticity, and second-order momentum compaction factor. Users can also introduce a skew quadrupole useful for emittance sharing and exchange studies. This paper describes the code structure, the physics models, and the algorithms used in CETASim. We also present the results of its application to the PETRA-IV storage ring.

1. Introduction

The 4th generation light sources move towards a diffraction-limited storage ring (DLSR) where the intense bunched beam with ultra-small emittance is stored for many hours for X-ray user operations. Because of the small beam dimensions with appreciable beam intensities, various collective effects will limit the performance of the ring in delivering the optimum beam parameters for user operations. Traditionally, the short- and long-range wakefield effects are the leading causes of instability that we must mitigate; however, we found that the ion, beam loading, transverse coupling, and other effects will also significantly impact the beam parameters. Since the Touschek lifetime impacts a whole aspect of operation, predicting and improving the lifetime becomes vital. These require investigating advanced beam dynamics caused by collective effects.

Multi-particle tracking has been a popular method to investigate the collective effects in the electron storage rings; various codes have been developed, including ELEGANT [1], MBTRACK [2], and PyHEADTAIL [3] *etc*. The benchmark between the codes is an ongoing effort in the light source communities. The motivation for developing CETASim is to have a light tool that includes the fundamental physics of various collective effects and approaches for instability mitigation. It is also beneficial for future studies since CETASim can be updated and upgraded appropriately when new physics needs arise. The remainder of this paper is organized as follows. In Section 2, the architecture of the code is introduced. Section 3 explains the physics models and algorithms for various collective effects used in CETASim. Section 4 showed simulation results when the code was used to study the PETRA-IV storage ring as a demonstration. A summary and conclusions are given at the end.

2. General code overview

We developed CETASim following object-oriented concepts in C++ programming language [4]. Fig. 1 shows the main classes designed in CETASim and a rough logical flow to set up the simulation. The program generates the specified bunch train and launches the particle tracking task using the input parameters in the run setup. For the multi-bunch problem, the users can set each bunch charge individually while keeping the number of macro-particles per bunch constant. It is a handy feature for investigating transient beam loading compensation and ion cleaning when head and tail bunches are set to accommodate a larger bunch charge (guarding bunches). CETASim can set multiple beam-ion interactions in the ring to investigate ion effects. At each interaction point, multiple ion species, local gas temperatures, and pressures can be set independently. The impedance class uses analytical formulas to construct the model impedance in a ring. At the current stage, two types of impedance elements, resistive wall, and resonator model, are available in CETASim. Meanwhile, CETASim can also import impedance data from an external file. The exciter class can set an external exciter to the electron bunches with a given frequency, which plays as a coupled

☆ Supported by the European Union's Horizon 2020 research and innovation program under grant agreement No. 871072.
* Corresponding author.
E-mail addresses: chao.li@desy.de (C. Li), yong-chul.chae@desy.de (Y.-C. Chae).

https://doi.org/10.1016/j.nima.2024.170031
Received 3 May 2024; Received in revised form 29 October 2024; Accepted 29 October 2024
Available online 3 November 2024

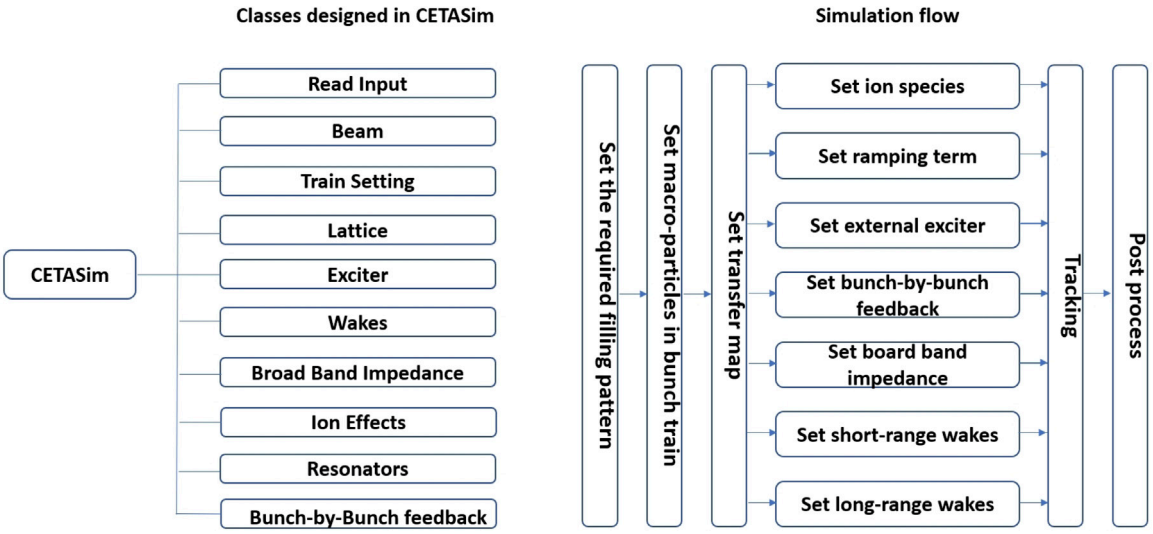

Fig. 1. General overview of CETASim code.

bunch mode driver in the "drive-damp" simulation. In a particular case of longitudinal coupled bunch motion, the resonator class deals with the transient beam loading effect. The cavity dynamics, driven by the generator current and the beam current, are simultaneously simulated in a self-consistent manner. We plan to implement cavity feedback to stabilize cavity voltage based on control parameters. The bunch-by-bunch feedback class adopts *Finite Impulse Response* (FIR) filter to compute the kicker response based on the multi-turn beam position monitor (BPM) data. The data output uses the SDDS format, which can be post-processed by the SDDS toolkit [5].

3. Physical models in CETASim

3.1. Particle convention in CETASim

In CETASim the position of every macro-particle is described by a 6D vector $\boldsymbol{x} = (x, p_x, y, p_y, dz, \delta)$ in phase space, where x and y are particle positions in the horizontal and vertical planes, p_x and p_y are the horizontal and vertical momentum normalized by the reference momentum p_0, dz and $\delta = (p - p_0)/p_0$ are the longitudinal positions and momentum deviation to the reference particle. The sign convention is such that the head of the particles has a positive distance, namely, $dz > 0$. If time-dependent elements are included, such as RF cavities, dz is converted to the time deviation by $d\tau = -dz/\beta c$ to compute the RF phase, where c is the speed of light, β is the ratio of particle nominal velocity to c.

3.2. Beam transfer in one turn

3.2.1. The longitudinal beam transformation

The longitudinal dynamics are described by

$$\begin{aligned} dz_{i+1} &= dz_i - L\sum_{j=1}^{3}\alpha_{cj}(\delta_i)^j \\ d\delta_{i+1} &= d\delta_i + \frac{1}{\beta^2 E_0}(-U_0 + \sum_n eV_{n,rf}\sin(\omega_{n,rf}d\tau_i + \phi_n)), \end{aligned} \tag{1}$$

where α_{cj} is the jth order of momentum compaction factor, E_0 is the nominal particle total energy, U_0 is the energy loss per turn due to the synchrotron radiation, n is the cavity index, $V_{n,rf}$, $\omega_{n,rf}$ and ϕ_n are the cavity voltage, angular frequency and phase respectively and e is the electron charge.

3.2.2. The transverse plane

In CETASim, users can split the ring into several sections. Then, the effect as beam-ion can be simulated with local lattice parameters several times instead of once per turn. In general, the beam transfer from the ith to the $(i+1)$th beam-ion interaction is represented by a symplectic map [6]

$$\boldsymbol{x_{i+1}} = \boldsymbol{H}_{i+1}^{-1}\boldsymbol{B}_{i+1}^{-1}\boldsymbol{M}_{i+1|i}\boldsymbol{B}_i\boldsymbol{H}_i\boldsymbol{x_i}. \tag{2}$$

$\boldsymbol{H}$ is the dispersion matrix

$$\boldsymbol{H} = \begin{pmatrix} \boldsymbol{I} & 0 & -\boldsymbol{H}_x \\ 0 & \boldsymbol{I} & -\boldsymbol{H}_y \\ -\boldsymbol{J_2}\boldsymbol{H}_x^T\boldsymbol{J_2} & -\boldsymbol{J_2}\boldsymbol{H}_y^T\boldsymbol{J_2} & \boldsymbol{I} \end{pmatrix}, \tag{3}$$

where

$$\boldsymbol{H}_x = \begin{pmatrix} 0 & \eta_x \\ 0 & \eta_x' \end{pmatrix}, \quad \boldsymbol{H}_y = \begin{pmatrix} 0 & \eta_y \\ 0 & \eta_y' \end{pmatrix}, \quad \boldsymbol{J}_2 = \begin{pmatrix} 0 & 1 \\ -1 & 0 \end{pmatrix}, \tag{4}$$

and $(\eta_x\ \eta_x', \eta_y\ \eta_y')$ are dispersion functions. $\boldsymbol{B} = (\boldsymbol{B}_x, \boldsymbol{B}_y, \boldsymbol{B}_z)$ and $\boldsymbol{M}_{i+1|i} = (\boldsymbol{M}_x, \boldsymbol{M}_y, \boldsymbol{M}_z)_{i+1|i}$ are the diagonal Twiss and rotation matrix that

$$\boldsymbol{B}_j = \begin{pmatrix} \frac{1}{\sqrt{\beta_j}} & 0 \\ \frac{\alpha_j}{\sqrt{\beta_j}} & \sqrt{\beta_j} \end{pmatrix}, \quad \boldsymbol{M}_{j,i+1|i} = \begin{pmatrix} \cos\psi_j & \sin\psi_j \\ -\sin\psi_j & \cos\psi_j \end{pmatrix}_{i+1|i}, \quad j = x, y, z, \tag{5}$$

where $\psi_{j,i+1|i}$ represents the phase advance between the ith and $(i+1)$th ring sections, α_j, β_j are the Twiss parameters. In CETASim, α_z and ψ_z are assumed to be zero, $\beta_z = \sigma_z/\sigma_e$, where σ_z and σ_e are the natural bunch length and energy spread.

CETASim also includes chromaticity and amplitude-dependent tune shift effects in simulation. Take the one-turn map for example and the one-turn phase advances are noted as $\psi_{(x,y)} = 2\pi\nu_{(x,y)}$, then the tunes applied in tracking are

$$\begin{aligned} \nu_x &= \nu_{x,0} + \xi_x\delta + \sum_{n=1}^{2}\left(\frac{\partial^n\nu_x}{\partial A_x^n}\frac{A_x^n}{n!} + \frac{\partial^n\nu_x}{\partial A_y^n}\frac{A_y^n}{n!}\right) + \frac{\partial^2\nu_x}{\partial A_x\partial A_y} \\ \nu_y &= \nu_{y,0} + \xi_y\delta + \sum_{n=1}^{2}\left(\frac{\partial^n\nu_y}{\partial A_x^n}\frac{A_x^n}{n!} + \frac{\partial^n\nu_y}{\partial A_y^n}\frac{A_y^n}{n!}\right) + \frac{\partial^2\nu_y}{\partial A_x\partial A_y} \end{aligned} \tag{6}$$

where $\nu_{(x,y),0}$ is the nominal tune, $\xi_{(x,y)}$ is the chromaticity, $A_{(x,y)}$ is the single particle oscillation amplitude

$$A_x = \frac{x_\beta^2 + (\alpha_x x_\beta + \beta_x x_\beta')^2}{\beta_x} \qquad A_y = \frac{y_\beta^2 + (\alpha_y y_\beta + \beta_y y_\beta')^2}{\beta_x}. \tag{7}$$

Noticeably, $(x_\beta\ x'_\beta)$ and $(y_\beta\ y'_\beta)$ in Eq. (7) are the particle betatron oscillation excluding the influence from the dispersion [1]. The derivation of $\nu_{(x,y)}$ reference to $A_{(x,y)}$ up to the second order has to be specified by the users in priori. Once the ring is separated into several sections in simulation, $\psi_{(x,y),i+1|i}$ can be obtained by Eq. (6) as well with a linear weighing $A_{(x,y),i+1|i}$ and $\xi_{(x,y),i+1|i}$.

3.2.3. Synchrotron radiation and quantum excitation

The synchrotron radiation and quantum excitation effect are simulated once per turn. In CETASim, We follow the approaches in Ref. [6] to simulate the synchrotron radiation and quantum excitation effects in the normalized frame $\boldsymbol{X} = \boldsymbol{BHx}$ according to

$$\begin{aligned}
\begin{pmatrix} \boldsymbol{X_1} \\ \boldsymbol{X_2} \end{pmatrix} &= \lambda_x \begin{pmatrix} \boldsymbol{X_1} \\ \boldsymbol{X_2} \end{pmatrix} + \sqrt{\epsilon_x(1-\lambda_x^2)} \begin{pmatrix} \hat{r}_1 \\ \hat{r}_2 \end{pmatrix} \\
\begin{pmatrix} \boldsymbol{X_3} \\ \boldsymbol{X_4} \end{pmatrix} &= \lambda_y \begin{pmatrix} \boldsymbol{X_3} \\ \boldsymbol{X_4} \end{pmatrix} + \sqrt{\epsilon_y(1-\lambda_y^2)} \begin{pmatrix} \hat{r}_3 \\ \hat{r}_4 \end{pmatrix} \\
\begin{pmatrix} \boldsymbol{X_5} \\ \boldsymbol{X_6} \end{pmatrix} &= \begin{pmatrix} 1 & 0 \\ 0 & \lambda_z^2 \end{pmatrix} \begin{pmatrix} \boldsymbol{X_5} \\ \boldsymbol{X_6} \end{pmatrix} + \begin{pmatrix} 0 \\ \sqrt{\epsilon_z(1-\lambda_z^4)} \end{pmatrix} \begin{pmatrix} 0 \\ \hat{r}_6 \end{pmatrix}.
\end{aligned} \tag{8}$$

Here $\hat{r}$ is an independent Gaussian random variable with a unit variance; $\lambda_{x,y,z} = \exp(-1/\tau_{x,y,z})$ is the transport coefficient with $\tau_{x,y,z}$ representing the synchrotron radiation damping time in the unit of the number of turns; ϵ_x, ϵ_y and ϵ_z are the equilibrium beam emittance, where $\epsilon_z = \sigma_z\sigma_e$. Once the synchrotron radiation and quantum excitation are done in the normalized frame $\boldsymbol{X}$, the physical vector $\boldsymbol{x}$ is recovered by $\boldsymbol{x} = \boldsymbol{H}^{-1}\boldsymbol{B}^{-1}\boldsymbol{X}$.

3.3. Impedance and wakes models in CETASim

The CETASim uses the broadband impedance in the frequency domain to simulate the single-bunch collective effect [7–9]. The coupled bunch effect is simulated in the time domain using the analytical formula of resistive wall and resonator wakes [7]. The impedance and wake data can be generated analytically or provided by users.

3.3.1. RLC impedance and wake

Eq. (9) gives the impedance of the RLC circuit as a function of angular frequency ω,

$$Z_m^{\parallel}(\omega) = \frac{\omega}{c} Z_m^{\perp}(\omega) = \frac{R_s}{1 + iQ(\frac{\omega_r}{\omega} - \frac{\omega}{\omega_r})}, \tag{9}$$

where R_s is the resistance with a dimension Ω/L^{2m}, Q is the quality factor, ω_r is the resonant angular frequency. Correspondingly, the longitudinal ($W'_m(z)$) and the transverse ($W_m(z)$) wake functions are

$$\begin{aligned}
W'_m(z) &= \begin{cases} 0 & z > 0 \\ \frac{R_s}{\tau_f} & z = 0 \\ 2\frac{R_s}{\tau_f} e^{z/c\tau_f}(\cos\frac{\bar{\omega}z}{c} + \frac{1}{\bar{\omega}\tau_f}\sin\frac{\bar{\omega}z}{c}) & z < 0, \end{cases} \\
W_m(z) &= \begin{cases} 0 & z = 0 \\ \frac{cR_s\omega_r}{2Q} e^{z/c\tau_f}\sin\frac{\bar{\omega}z}{c} & z \le 0, \end{cases}
\end{aligned} \tag{10}$$

where $\tau_f = 2Q/\omega_r$ represents the filling or damping time in the circuit, $\bar{\omega} = \sqrt{\omega_r^2 - 1/\tau_f^2}$. $-z/c$ represents the time passed by referenced to the δ impulse at the impedance element.

3.3.2. Resistive wall impedance and wake

The resistive wall (RW) impedance from an infinitely thick metallic beam pipe of radius b and conductivity σ is well-known [7]. For an elliptical beam pipe, the code uses Yokoya's form factors [10] to account for the ellipticity. Eq. (11) shows the model of RW impedance per unit length as a function of angular frequency ω

$$\begin{aligned}
\frac{Z_m^{\parallel}(\omega)}{L} = \frac{\omega}{c}\frac{Z_m^{\perp}(\omega)}{L} &= \frac{4/b^{2m}}{(1+\delta_{m0})bc\sqrt{\frac{2\pi\sigma}{|\omega|}} - \frac{ib^2}{m+1}\omega + \frac{imc^2}{\omega}} \\
&\approx \sqrt{\frac{2}{\pi\sigma}}\frac{1}{(1+\delta_{m0})b^{2m+1}c}|\omega|^{1/2}[1 - sgn(\omega)i],
\end{aligned} \tag{11}$$

where $\delta_{m,0}$ is the Kronecker-Delta function, i is the imaginary unit, sgn is the $Sign$ function. Limiting the RW impedance to the lowest orders $m = 0, 1$ in the longitudinal and transverse, respectively, the longitudinal and transverse wake functions can be obtained by Fourier transformation. Define $z_0 = (2\chi)^{1/3}b$ as the characteristic distance, where $\chi = c/(4\pi\sigma b)$ is a dimensionless parameter, the longitudinal and transverse RW wakes are [2]:

$$\begin{aligned}
W'_0(z) &= \frac{1}{b^2}[\frac{e^{z/z_0}}{3}\cos(\frac{\sqrt{3}z}{z_0}) - \frac{\sqrt{2}}{\pi}\int_0^\infty dx\frac{x^2e^{x^2z/z_0}}{x^6+8}] \\
W_1(z) &= \frac{32}{b^3}(2\chi)^{1/3}[-\frac{e^{z/z_0}}{12}\cos(\frac{\sqrt{3}z}{z_0}) - \frac{1}{4\sqrt{3}}e^{z/z_0}\sin(\frac{\sqrt{3}z}{z_0}) \\
&\quad + \frac{\sqrt{2}}{\pi}\int_0^\infty dx\frac{e^{x^2z/z_0}}{x^6+8}].
\end{aligned} \tag{12}$$

If the simplified RW impedance in Eq. (11) is adopted, the RW wakes exhibit the usual long-range formula

$$W'_0(z) \approx \frac{1}{2\pi b}\sqrt{\frac{c}{\sigma}}\frac{1}{|z|^{3/2}} \qquad W_1(z) \approx -\frac{2}{\pi b^3}\sqrt{\frac{c}{\sigma}}\frac{1}{|z|^{1/2}}. \tag{13}$$

Fig. 2 compares the exact and approximate solution of the RW impedance and wakes. In terms of impedance, the discrepancy exists both in the low and high-frequency regions. The results from the exact and the approximated solutions are the same in the medium frequency region. The wakes from the exact and approximate solutions agree well when $u = z/z_0 > 5$. Since the distance among different bunches is much longer than the characteristic distance z_0, the asymptotic wake Eq. (13) is used in CETASim for the coupled-bunched simulation to relax the computation load.

3.4. Single bunch effect

The energy change within the bunch caused by the longitudinal wake or impedance can be expressed as

$$eV^{\parallel}(z) = -e\int_z^\infty \rho(z')W'_0(z-z')dz' = -\frac{e}{2\pi}\int_{-\infty}^\infty e^{i\omega z/c}\tilde{\rho}(\omega)Z_0^{\parallel}(\omega)d\omega, \tag{14}$$

where $\tilde{\rho}(\omega)$ is the charge-density spectrum in frequency domain. In the transverse plane, we consider the dipole W_1^D and quadrupole W_1^Q wakes, the impedance of which is denoted as $Z_1^D(\omega)$ and $Z_1^Q(\omega)$ respectively. The transverse kick from the impedance within the bunch can be expressed as

$$\begin{aligned}
eV^{\perp}(z) &= -e\int_z^\infty \rho(z')x(z')W_1^D(z-z')dz' \\
&\quad - e\int_z^\infty \rho(z')x(z)W_1^Q(z-z')dz' \\
&= -i\frac{e}{2\pi}\int_{-\infty}^\infty e^{i\omega z/c}\tilde{\rho}^D(\omega)Z_1^D(\omega)d\omega \\
&\quad - i\frac{e}{2\pi}x(z)\int_{-\infty}^\infty e^{i\omega z/c}\tilde{\rho}(\omega)Z_1^Q(\omega)d\omega,
\end{aligned} \tag{15}$$

where, $x(z)$ is the transverse position offset along the beam, $\tilde{\rho}^D(\omega)$ is the spectrum of the dipole moment $\rho(z)x(z)$.

Noticeably, in simulation, it is always recommended to ensure the number of macro-particles is large enough to sample the longitudinal bunch profile $\rho(z)$ correctly, which significantly increases the computation load. In CETASim, a Gaussian filter is applied to smooth the longitudinal profile when the number of the macro-particles is not large enough. Care has to be taken on this point when benchmarks are launched among different simulation codes.

For a given impedance, Eqs. (14) and (15) in frequency domain, are used to compute $eV^{\parallel}(z)$ and $eV^{\perp}(z)$ in CETASim. In the future, if there is a requirement to do the simulation with the time domain method, a subroutine can be developed to import the wakes from an external file supplied by the user to get $eV^{\parallel}(z)$ and $eV^{\perp}(z)$ as well.

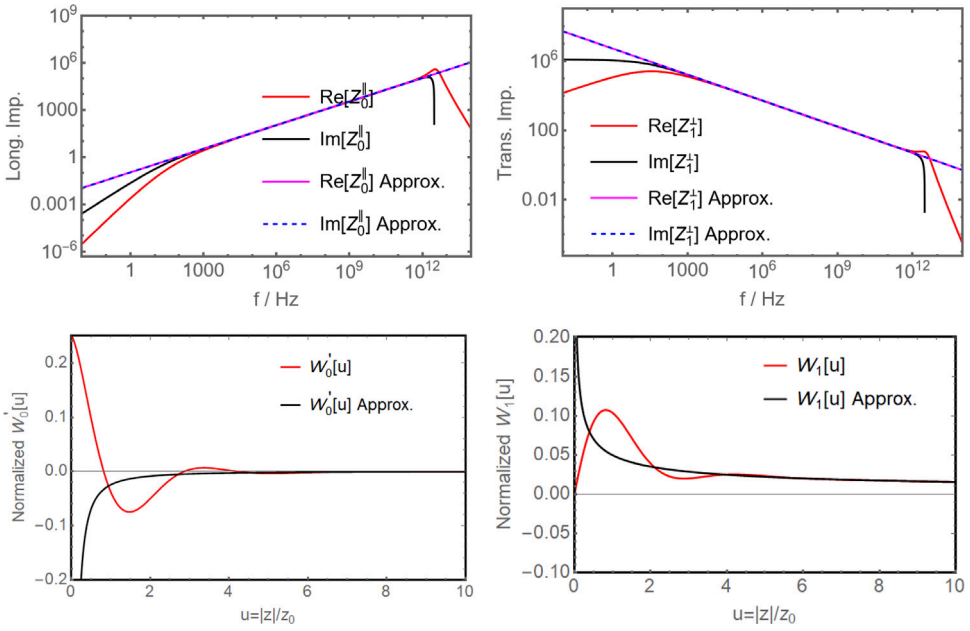

Fig. 2. Comparison of the exact and approximated solutions of the resistive impedance (above) and wakes (bottom). The sub-figures on the left and right correspond to the longitudinal ($m = 0$) and the transverse ($m = 1$) respectively.

3.5. Coupled bunch effect

If the wakes are generated by the RW or high-Q resonators, which last longer than the bunch spacing, the motion of the bunches will be coupled. Assuming there are N_b bunches in the ring, the kick at the jth bunch at the nth turn from the longitudinal wakes W_0' and transverse dipole (W_1^D) and quadrupole wakes (W_1^Q) can be expressed as

$$\begin{aligned}
\Delta p^j_{z;n} &\sim \sum_{k=0}^{n-1}\sum_{i=0}^{Nb-1} W_0'(hcT_{rf}(n-k)+\delta s_{i;j}) \\
\Delta p^j_{x;n} &\sim \sum_{k=0}^{n-1}\sum_{i=0}^{Nb-1} [\langle x\rangle^i_k W_1^D(hcT_{rf}(n-k)+\delta s_{i;j}) \\
&\quad + \langle x\rangle^j_0 W_1^Q(hcT_{rf}(n-k)+\delta s_{i;j})], \\
\delta s_{i;j} &= \begin{cases} (i-j)cT_{rf} & j \le i \\ (i-j+h)cT_{rf} & j > i \end{cases}
\end{aligned} \tag{16}$$

where h is the RF harmonic number, T_{rf} is the RF period, $\langle x\rangle^i_k$ is bunch centroid of the ith bunch at kth previous turn. CETASim can simulate the long-range wakes from the RW (Eq. (10)) and RLC (Eq. (13)) elements. The user can specify the wake length in the number of turns.

3.6. Bunch-by-bunch feedback

The bunch-by-bunch feedback can mitigate the coupled bunch instabilities. It detects the transverse or longitudinal positions and creates the kicker signal for each bunch. A digital FIR filter to process the position signal into the kicker strength is expressed as

$$\Theta_n = \sum_{k=0}^{N} a_k \theta_{n-k} \tag{17}$$

where a_k represents the filter coefficient, θ_{n-k} and Θ_n are the input and output of the filter. The number of the input data $N + 1$ is defined as taps of the filter. With a given coefficient, the bunch momentum change at the kicker in the nth turn due to the bunch-by-bunch feedback can be found

$$\begin{aligned}
&\Delta p_{x;n} \sim K_x \sum_{k=0}^{N} a_{k,x}\langle x\rangle_{n-k}, \quad \Delta p_{y;n} \sim K_y \sum_{k=0}^{N} a_{k,y}\langle y\rangle_{n-k}, \\
&\Delta \delta_n \sim K_z \sum_{k=0}^{N} a_{k,z}\langle z\rangle_{n-k},
\end{aligned} \tag{18}$$

where $\langle x, y, z\rangle_{n-k}$ is the bunch centroids of the kth previous turn at the BPM, $K_{x,y,z}$ is the gain factor. Particles in one bunch experience the same kick. The shunt impedance and power constraint of the kicker, specified by the users, limit the maximum kick strength experienced by particles.

3.7. Beam-ion effect

CETASim simulates the Coulomb interaction between the electron bunch and the ionized gases [11]. In accelerators, if the gas pressure P, gas temperature T, and ionization collision cross-section Σ are given, the number of ionized ions can be obtained by

$$\Lambda = \Sigma \frac{PN_A}{RT} N_b, \tag{19}$$

where N_b is the number of electron particles, R the ideal gas constant and N_A is the Avogadro constant. The ions can be locally trapped by passing electron bunches acting as the focusing lenses. The trapping condition is

$$A \ge A_c = \frac{QN_b r_p \Delta T_b c}{2\sigma_y(\sigma_x + \sigma_y)} \tag{20}$$

where A is the ion mass, Q is the ion charge number, r_p is the classical radius of the proton, ΔT_b is the bunch separation in time. Only the ions with a mass number larger than the critical mass number A_c can be trapped. This formula assumes a linear focusing and uniform fill pattern. Note that the critical ion mass A_c varies following the betatron functions around the ring.

In CETASim, we assume the electron bunch has a rigid Gaussian distribution. The *Bassetti − Erskine* formula [12] is applied at the

interaction point s_i to get the beam ion interaction force

$$\boldsymbol{F}_{y(x,y)} + i\boldsymbol{F}_{x(x,y)} = \delta(s_i)\sqrt{\frac{\pi}{2(\sigma_x^2-\sigma_y^2)}} \{w(\frac{x+iy}{\sqrt{2\pi(\sigma_x^2-\sigma_y^2)}}) - \exp(-\frac{x^2}{2\sigma_x^2}-\frac{y^2}{2\sigma_y^2})w(\frac{x\frac{\sigma_y}{\sigma_x}+iy\frac{\sigma_x}{\sigma_y}}{\sqrt{2\pi(\sigma_x^2-\sigma_y^2)}})\}, \tag{21}$$

where $w(z)$ is the complex error function, σ_x and σ_y are the rms bunch size [13]. Note N_i as ionized ions; the motions of electrons and ions follow the equation [14]

$$\frac{d^2\langle \boldsymbol{x}\rangle}{ds^2} = \frac{2r_e}{\gamma}\sum_{i=0}^{N_i}\boldsymbol{F}(\langle \boldsymbol{x}\rangle - \boldsymbol{X}_i), \qquad \frac{d^2\boldsymbol{X}_i}{dt^2} = \frac{2N_b r_e c^2}{M_i/m_e}\sum_{j=0}^{N_b}\boldsymbol{F}(\boldsymbol{X}_i - \langle \boldsymbol{x}\rangle), \tag{22}$$

where $\boldsymbol{X_i} = (x,y)_i$ is the ion position, $\langle \boldsymbol{x}\rangle = (\langle x\rangle, \langle y\rangle)$ is the electron bunch centroids, $\boldsymbol{F}$ is the Coulomb force between the ions and electrons, r_e is the classical electron radius, γ is the relativistic factor of electron beam, M_i and m_e are the mass of ion and electron. This model assumes that the electron bunch rigid follows Gaussian distribution (weak–strong model) with centroid oscillation. CETASim also supplies a subroutine assuming that ion distribution follows the Gaussian profile as well. Then the motion of individual electrons kicked by the ions can be simulated in a similar way (quasi-strong–strong model). This method is not physically correct, since ions normally do not follow the Gaussian shape, however, it can give a first glance of incoherent electron particle behavior in simulation.

3.8. Beam loading effect and cavity feedback

The longitudinal dynamics due to the cavity's RF mode can also be simulated. CETASim follows the algorithm in P.B. Wilson's paper [15], where the beam-induced voltage is treated in the phasor frame. The force electron experiences in terms of beam-included voltage in the phasor fame are equivalent to the force in terms of the long-range wake. However, in the phasor frame, the history of the bunches in previous turns is no longer needed, reducing the computation load significantly.

The transient beam loading effect particularly refers to the fundamental cavity mode, which is the same mode building up the acceleration field. By modeling the fundamental mode of the cavity as an RLC circuit, the generator dynamics and beam dynamics are coupled. In a ring with multiple RF systems, at least the main cavity has to be active, which brings additional complexity to the whole study, especially when the cavity feedback has to be included further.

In the RLC circuit model, note the driven current as $\tilde{\boldsymbol{I}}(t)$ in general, the voltage excited $\tilde{\boldsymbol{V}}(t)$ follows the differential equation [16]

$$\frac{d^2}{dt^2}\tilde{\boldsymbol{V}}(t) + \frac{\omega_r}{Q_L}\frac{d}{dt}\tilde{\boldsymbol{V}}(t) + \omega_r^2\tilde{\boldsymbol{V}}(t) = \frac{\omega_r R_L}{Q_L}\frac{d}{dt}\tilde{\boldsymbol{I}}(t), \tag{23}$$

where ω_r, Q_L and R_L are the circuit angular resonant frequency, the loaded quality factor and the shunt impedance respectively.

Note ω_{rf} as the angular frequency of the driving term $\tilde{\boldsymbol{I}}(t)$, if several conditions are met: (1) the second-order terms can be neglected; (2) $Q_L \gg 1$; (3) $\Delta\omega = \omega_r - \omega_{rf} \ll \omega_r$, and together with the zero-order hold method [16,17], the solution of Eq. (23) can be further simplified in the state space

$$\begin{pmatrix}\Re\tilde{\boldsymbol{V}}\\ \Im\tilde{\boldsymbol{V}}\end{pmatrix}_{t+\Delta t} = e^{-\omega_{1/2}\Delta t}\begin{pmatrix}\cos\Delta\omega\Delta t & -\sin\Delta\omega\Delta t\\ \sin\Delta\omega\Delta t & \cos\Delta\omega\Delta t\end{pmatrix}\begin{pmatrix}\Re\tilde{\boldsymbol{V}}\\ \Im\tilde{\boldsymbol{V}}\end{pmatrix} + \frac{\omega_r R_L}{2Q_L(\omega_{1/2}^2+\Delta\omega^2)}\begin{pmatrix}A & B\\ -B & A\end{pmatrix}\begin{pmatrix}\Re\tilde{\boldsymbol{I}}\\ \Im\tilde{\boldsymbol{I}}\end{pmatrix}_t \tag{24}$$

where $\Re$ and $\Im$ represent the real and imaginary part of the phasor, $\omega_{1/2} = 1/\tau_f$, Δt is the time step, A and B are

$$A = \Delta\omega e^{-\omega_{1/2}\Delta t}\sin\omega_{1/2}\Delta t - \omega_{1/2}e^{-\omega_{1/2}\Delta t}\cos\omega_{1/2}\Delta t + \omega_{1/2}$$
$$B = \omega_{1/2}e^{-\omega_{1/2}\Delta t}\sin\omega_{1/2}\Delta t + \Delta\omega e^{-\omega_{1/2}\Delta t}\cos\omega_{1/2}\Delta t - \Delta\omega. \tag{25}$$

In CETASim, the current $\tilde{\boldsymbol{I}}(t)$ is splitted into two parts, the generator current $\tilde{\boldsymbol{I}}_g(t)$ and beam current $\tilde{\boldsymbol{I}}_b(t)$ [18], which drive the generator voltage $\tilde{\boldsymbol{V}}_g(t)$ and beam-induced voltage $\tilde{\boldsymbol{V}}_b(t)$ respectively. The total cavity voltage that beam can sample as a function of time t is

$$\tilde{\boldsymbol{V}}_c(t) = \tilde{\boldsymbol{V}}_g(t) + \tilde{\boldsymbol{V}}_b(t). \tag{26}$$

Since the generator current $\tilde{\boldsymbol{I}}_g(t)$ is continuous, for a given initial driving current $\tilde{\boldsymbol{I}}_g(\boldsymbol{0})$, Eq. (24) is numerically solved by CETASim to obtain $\tilde{\boldsymbol{V}}_g(t)$ step by step in the time domain. It is referenced as the generator dynamics. Moreover, Eq. (24) is still valid even when there exists feedback current $\delta\tilde{\boldsymbol{I}}_g(\boldsymbol{t})$.

Unlike $\tilde{\boldsymbol{I}}_g(t)$, the beam current (bunched beam train) $\tilde{\boldsymbol{I}}_b(t)$ is discrete which can be expressed as

$$\tilde{\boldsymbol{I}}_b(t) \propto \sum_{k=-\infty}^{k=\infty}\delta(t-kT_{rf}) = I_{DC} + 2I_{DC}\sum_{k=1}^{k=\infty}\exp(ik\omega t), \tag{27}$$

where I_{DC} is the DC component of beam current. Noticeably, only the frequency component at ω_{rf} is synchronized with the bunch repetition rate so that the driving current due to the beam can be further simplified to $-2I_{DC}\exp(i\omega_{rf}t)$. In principle, the beam-induced voltage $\tilde{\boldsymbol{V}}_b(t)$ can be obtained by solving Eq. (23) as well. However, this procedure can be significantly simplified from the fundamental theory of beam loading. Assume there is a bunch with charge q passing through the cavity at time $t-\Delta t$, then the beam-induced voltage follows

$$\tilde{\boldsymbol{V}}_b(t) = (\tilde{\boldsymbol{V}}_b(t-\Delta t) + \tilde{\boldsymbol{V}}_{b0}/2)\exp(\alpha\Delta t), \quad \alpha = -\frac{1}{\tau_f}(1 - i\tan\Psi) \tag{28}$$

where Ψ is the cavity de-tuning angle. The phase and amplitude of the beam induced voltage $\tilde{\boldsymbol{V}}_{b0}/2$ is π and $|\tilde{\boldsymbol{V}}_{b0}| = q\omega_r R_L/Q_L$. Eq. (28) shows that the accumulated beam-induced voltage $\tilde{\boldsymbol{V}}_b(t)$ adds an impulse $\tilde{\boldsymbol{V}}_{b0}/2$ whenever a charged bunch passes by, then decays and rotates by a factor of $\exp(\alpha\Delta t)$ until the next bunch comes. The information on the bunches at previous turns is not needed.

Noticeably, if there exist longitudinal beam offsets, the total cavity voltage [19] each bunch samples usually deviate from the designed value due to the beam-induced voltage, especially when the ring is filled non-uniformly,

$$\tilde{\boldsymbol{V}}_c(t) = \tilde{\boldsymbol{V}}_g(t) + \tilde{\boldsymbol{V}}_b(t) \neq V_c^{set}\exp(i\omega_{rf}t + \phi). \tag{29}$$

Thus, cavity feedback is required to compensate for the transient beam-loading effect. Fig. 3 shows a loop of cavity feedback at the generator side. The performance of the cavity feedback systems is determined by the measured cavity phasor $\tilde{\boldsymbol{V}}_c(t)$ at times $t = nT_{rf}$, which is multiple of the RF cycle. The cavity feedback filter could be a *Finite Impulse Response* (FIR) or a *Infinite Impulse Response* (IIR) types, which takes the generator current deviation $\delta\tilde{\boldsymbol{I}}_g(t)$ and cavity voltage error $\delta\tilde{\boldsymbol{V}}(t) = \tilde{\boldsymbol{V}}_c^{set}(t) - \tilde{\boldsymbol{V}}_c(t)$ as input and gives $\delta\tilde{\boldsymbol{I}}_g(t)$ to be modified at the generator side as output. At the time nT_{rf}, the addition generator current can be expressed explicitly as

$$\delta\tilde{\boldsymbol{I}}_g(nT_{rf}) = -\frac{1}{a_0}\sum_{i=1}^{N}a_i\delta\tilde{\boldsymbol{I}}_g((n-i)T_{rf}) + \frac{1}{b_0}\sum_{j=0}^{M}b_j\delta\tilde{\boldsymbol{V}}_c((n-j)T_{rf}), \tag{30}$$

where a_i and b_j are coefficients of filters, N and M are the orders of the filters.

Finally, we summarize the steps for the transient beam loading and cavity feedback simulation in one turn,

1. Solve Eq. (24) with a given $\tilde{\boldsymbol{I}}_g(0)$ to get the $\tilde{\boldsymbol{V}}_g(t)$;
2. Solve Eq. (28) to get the $\tilde{\boldsymbol{V}}_b(t)$;
3. Solve Eq. (29) to get the $\tilde{\boldsymbol{V}}_c(t)$;
4. Transfer the particle by the one-turn map;
5. Solve Eq. (30) to get the $\delta\tilde{\boldsymbol{I}}_g(t)$.

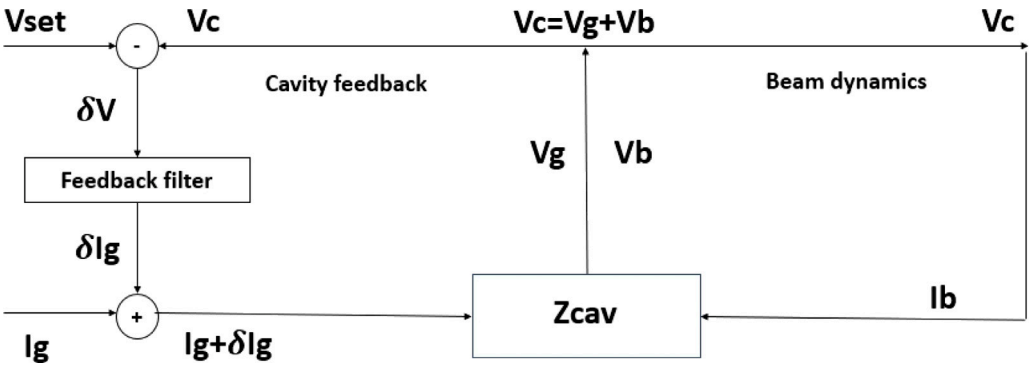

Fig. 3. Interaction between generator dynamics, beam dynamics, and cavity feedback.

Table 1
Nominal lattice parameters of PETRA-IV H6BA lattice [20].

Parameters	Units	Symbol	DW closed	DW open
Energy	GeV	E	6	6
Circumference	m	C	2304	2304
Natural emittance	pm	ϵ_0	20	43
Emittance ratio		κ	0.1	0.1
Tunes		ν_x/ν_y	135.18/86.27	135.18/86.23
Momentum compact factor		α_c	3.33×10^{-5}	3.33×10^{-5}
Damping time	ms	τ_x	17.76	39.23
Damping time	ms	τ_y	22.14	69.63
Damping time	ms	τ_s	12.62	56.84
Natural energy spread	rad	σ_E	8.9×10^{-4}	7.37×10^{-4}
Natural bunch length	mm	σ_s	2.3	1.794
Energy loss	MeV	U_0	4.166	1.423
Main cavity voltage	MV	$V_{c,1}$	8	8
Main cavity harmonics		h	3840	3840

Two more points to be emphasized: (1), The algorithm assumed a zero bunch length. This approximation is not appropriate for a bunch with a finite length. In that case, the bunch can be cut into bins in the time sequence, and each bin can be treated as zero-length micro-bunches. (2), if multi-cavities are included in the system, CETASim applies the same procedure to simulate the generator dynamics, beam dynamics and cavity feedback for each cavity sequentially.

4. CETASim benchmarks and implementation

We take the H6BA lattice of the PETRA-IV storage ring [20] as the test bed to show the capability of CETASim. Table 1 shows the main lattice parameters. PETRA-IV will adopt an active 3rd harmonic cavity to lengthen the bunch. The ideal bunch lengthening condition requires $\Re(\tilde{V}_c(\tau = 0)) = U_0/e$ to compensate the radiation loss U_0, $\Re(\tilde{V}_c'(\tau = 0)) = \Re(\tilde{V}_c''(\tau = 0)) = 0$ to have a flat RF potential. For collective effect, we use the RW impedance and the geometric impedance. The insertion device (ID) chambers contribute more to the RW impedance than the ring chambers. The geometrical impedance is due to the elements in the ring such as BPMs, Bellows, Flanges, *etc*. The program ImpedanceWake2D [21] is used to compute the resistive wall impedance. GdfidL computes the geometric wake potentials [22], where a 1 mm long Gaussian bunch is used as the driving bunch. Fig. 4 shows the wake potential in the longitudinal, horizontal, and vertical planes of a 1-mm Gaussian bunch and its impedance. Here, the transverse wake potential and impedance are multiplied by the average betatron function $\langle\beta\rangle$ so that the unit differs from conventional ones.

4.1. Beam equilibrium state with zero beam current

As a first step, we check the algorithm by demonstrating the effects of radiation damping and quantum excitation. We prepare one bunch with an initial Gaussian distribution in the longitudinal and transverse phase space with 3×10^4 macro-particles. The initial condition of the bunch is with the emittance $\epsilon_{x,0} = \epsilon_{y,0} = 10$ pm, the energy spread $\sigma_{E,0} = 8.9 \times 10^{-4}$ rad, and the bunch length $\sigma_{z,0} = 5.3 \times 10^{-3}$ m. The emittance ratio κ is set as 0.1. The radiation damping times shown in Table 1 [20] are applied in simulation. Fig. 5 shows how the bunch length, energy spread, and transverse emittance evolve as a function of tracking turns. The beam evolves into the natural equilibrium state as expected.

4.2. Single bunch effect

With the broadband impedance shown in Fig. 4, we study the single-bunch effects [23]. The longitudinal impedance leads to potential well distortion and bunch lengthening effects. Once the single bunch current increases and the longitudinal microwave instability threshold is reached, the energy spread also increases. We compare two RF configurations, namely, the main cavity only and the main cavity with a 3rd harmonic cavity. With the harmonic system, the generator voltage and phase are set to maintain the ideal bunch lengthening condition. Fig. 6 shows the single bunch length and energy spread as a function of the bunch current. In each sub-figure, two groups of curves are given. The red ones are from CETASim and the black ones are from Elegant. The bunch length given by CETASim agrees well with the results given by Elegant. We notice some discrepancies in the energy spread above the microwave instability threshold. It could be derived from different types of filters for longitudinal profile smoothing purposes.

In the transverse plane, the impedance leads to the Transverse Mode Coupling Instability (TMCI) and head–tail instabilities. The azimuthal modes shift as the single bunch current increases. At a certain point, these azimuthal modes start to overlap and merge; then the beam becomes unstable. If there exists dipole impedance only, this mode coupling condition can be studied analytically through Sacherer's method [7]. Applying this method, one can set up a group of integral equations and solve it consistently to get the mode-coupling condition–Vlasov solver. We set the simulation with zero chromaticity as a benchmark study and only considered the vertical dipole impedance. The comparison of the azimuthal mode frequency shift between CETASim tracking and the Vlasov solver in CETA [24] code package is shown in Fig. 7. The black dots and contours represent the Vlasov solver and CETASim results respectively. The contour represents the strength of the oscillation modes in the logarithmic scale. The results from CETASim simulation are consistent with the predictions from the Vlasov solver, showing that the TMCI beam current threshold is around 0.11 mA.

One way to increase the transverse single-bunch current limit is to set a non-zero chromaticity ξ. The chromaticity introduces a head–tail phase advance and shifts the mode spectrum by $\omega_\xi = \xi f_0/\eta$, where η is the lattice slip factor, and f_0 is the nominal revolution frequency.

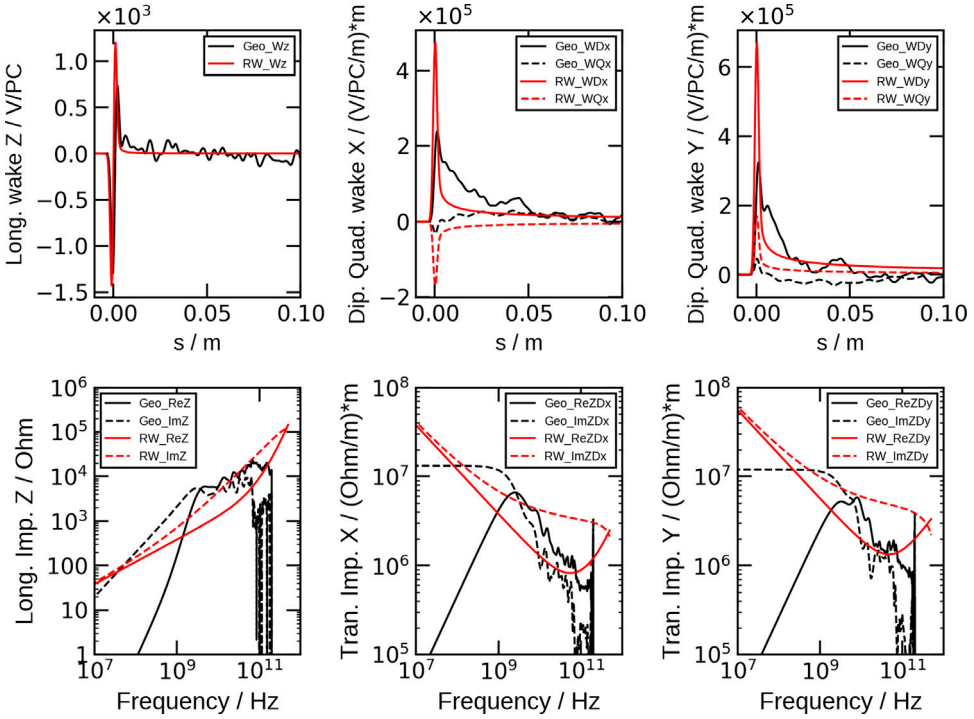

Fig. 4. Top: wakes of a 1 mm leading electron Gaussian bunch due to the geometrical impedance and the resistive wall impedance. Bottom: the geometrical impedance and the resistive wall impedance. From left to right, figures correspond to the longitudinal, horizontal, and vertical directions, respectively. The quadruple impedance is not plotted here.

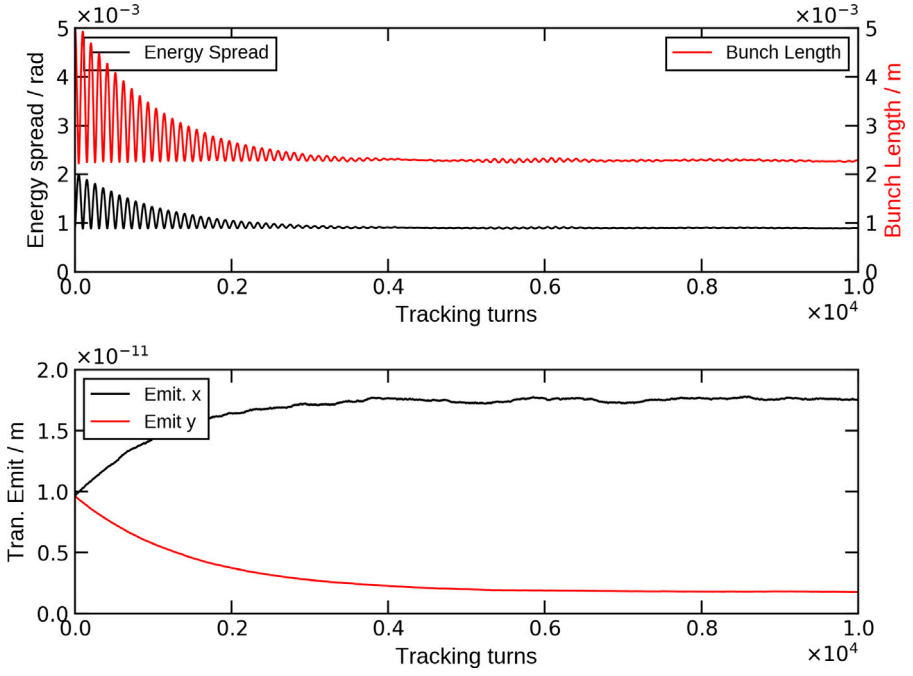

Fig. 5. Bunch energy spread, bunch length (top), and transverse beam emittance (bottom) as a function of tracking turns. The beam evolves to the natural equilibrium state as expected. The macro-particle number is set as 3×10^4 in the simulation.

Fig. 8 shows the single bunch current limit as a function of chromaticity without and with 3rd harmonic cavity. The transverse dipole, quadrupole impedance, and longitudinal impedance are all considered in the simulation. The threshold current is the lowest bunch current, with zero particle loss at the elliptic aperture of $(a, b) = (15, 10)$ mm. The macro-particle number is set as 3×10^4 in the simulation.

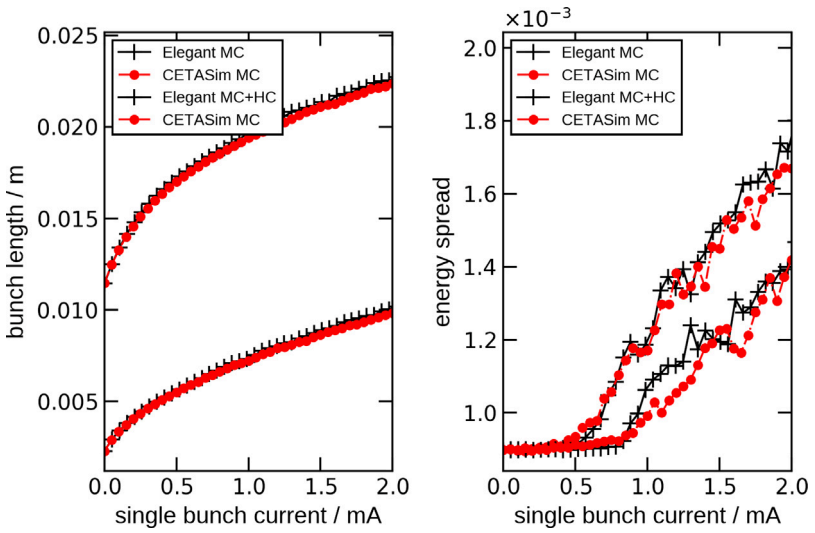

Fig. 6. Single bunch length (left), energy spread (right) as a function of bunch current.

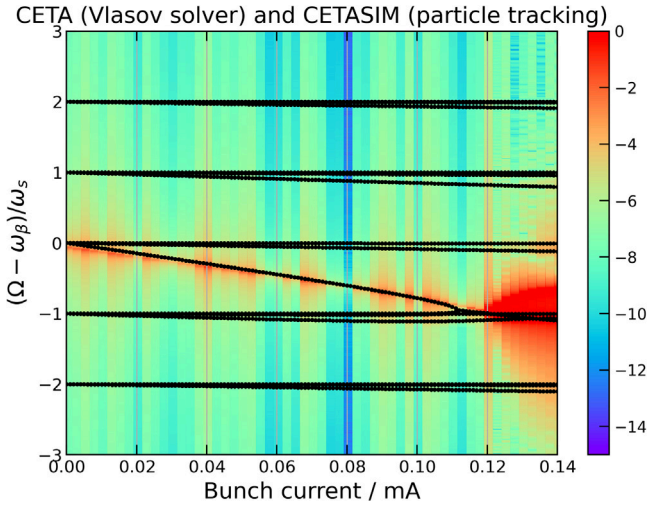

Fig. 7. Comparison of the TMCI threshold from Vlasov solver (black dots) and CETASim (contours). The contour represents the strength of the oscillation modes in the logarithmic scale. In tracking, only the vertical dipole impedance is taken into account.

4.3. Coupled-bunch instability due to the long-range wakes

The frequency shift of multi-bunch coherent modes can be expressed as

$$(\Omega^\mu-\omega_\beta)_\perp=-i\frac{MNr_0c}{2\gamma T_0^2\omega_\beta}\sum_{p=-\infty}^{\infty}Z_1^\perp[\omega_\beta+(pM+\mu)\omega_0]$$
$$(\Omega^\mu-\omega_s)_\parallel=i\frac{MNr_0\eta}{2\gamma T_0^2\omega_s}\sum_{p=-\infty}^{\infty}(\omega_s+pM\omega_0+\mu\omega_0)Z_0^\parallel[\omega_s+pM\omega_0+\mu\omega_0], \tag{31}$$

where M is the number of equal spaced bunch number, N is the electron particle number per bunch, μ is the coupled bunch mode index varying from 0 to M-1, ω_β and ω_s are the transverse and longitudinal oscillation angular frequency. The coupled bunch mode can be reconstructed in particle tracking studies when the bunch-by-bunch and turn-by-turn data are available. Take the horizontal plane, for example; the coupled bunch mode can be obtained from the Fourier spectrum of the one-turn complex signal z_μ at a certain BPM

$$z_\mu=(\frac{x_\mu}{\sqrt{\beta_x}}-i(\sqrt{\beta_x}p_{x,\mu}+\frac{\alpha_x}{\sqrt{\beta_x}}x_\mu))e^{-i\frac{2\pi\nu_x(\mu-1)}{M}}, \tag{32}$$

where β_x and α_x are the Twiss parameters at the BPM. The growth rate of the μth mode can be obtained by an exponential fitting of the μth mode spectrum amplitude as a function of tracking turns.

However, in a real machine, what can be measured at the BPM is limited to only position information. Hence, CETASim follows the method of the drive-damp experiment to get the coupled bunch instability growth rate [25]. A driver can be set in CETASim to excite the beam with a given kick strength and frequency f_μ by which the μth coupled bunch mode can be excited. Then the signal

$$\tilde{S}_n^\mu=\sum_{m=0}^{M}\tilde{s}_{n,m}^\mu=\sum_{m=0}^{M}x_{n,m}\exp(-i2\pi f_\mu hT_{rf}/M), \tag{33}$$

is recorded turn by turn. The growth rate of the excited μth mode can be found by an exponent fitting of $|\tilde{S}_n^\mu|$. Then, one can reconstruct the full picture of the coupled-bunch mode by scanning the driver's driving frequency f_μ.

CETASim has two analytical models to generate the long-rang wakes: the RLC model and the RW model. Below, two examples are given for the transverse coupled bunch effect study. In the first case, the transverse impedance modeled by an RLC resonator with the parameters $R_s=5\times10^9\ \Omega/\mathrm{m}^2$, $Q=1\times10^{-3}$ and $\omega_r=2\pi\times4.996\times10^8$ 1/s. The second one is a simplified resistive wall impedance of the PETRA-IV storage ring, where the vacuum chamber is grouped into 4 types of sections as shown in Table 2. The characteristic distance z_0 of these four sections are in the order of $1.\times10^{-5}$ m, which is much smaller than the RF bucket distance $cT_{rf}=0.6$ m, so that Eq. (13) applied in CETASim is still a good approximation. In the simulation, the ring is filled uniformly by 80 bunches, and each bunch has a current of 1 mA. The long-range wakes are truncated at the 20th turn in this study, which is chosen as a compromise between simulation speed and accuracy. Meanwhile, this 20 turns long-range wake applied here also ensures the coupled bunch mode growth rate simulation converged as well. In Fig. 9, we give the results of the coupled bunch mode growth rate from CETASim tracking ('Ideal') and analytical predictions ('Prediction'). These agree well with each other. In this simulation study, the synchrotron radiation damping is turned off.

Fig. 10 represents the coupled bunch modes reconstructed from the drive-damp method. The driving strength of the exciter is 0.2 μrad,

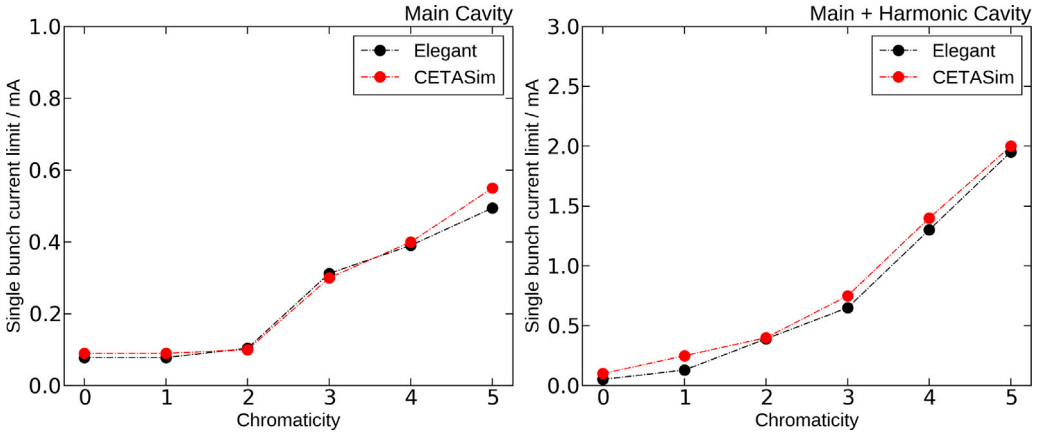

Fig. 8. The single bunch current threshold as a function of chromaticity without (left) and with (right) the 3rd harmonic cavity. The macro-particle number is set as 3×10^4 in the simulation.

Table 2
Simplified resistive wall sections in PETRA-IV.

Section	Number	len./m	gaps/mm	β_x/m	β_x/m	Conduct. σ/Ω^{-1} m^{-1}	z_0/m
5 mm ID	4	5	5	3.14	3.14	2.5×10^7	1.74×10^{-5}
6 mm ID	17	5	6	3.14	3.14	2.5×10^7	1.97×10^{-5}
7 mm ID	5	10	7	6.08	6.08	2.5×10^7	2.18×10^{-5}
ring	1	2149	20	2.71	4.25	5.9×10^7	2.08×10^{-5}

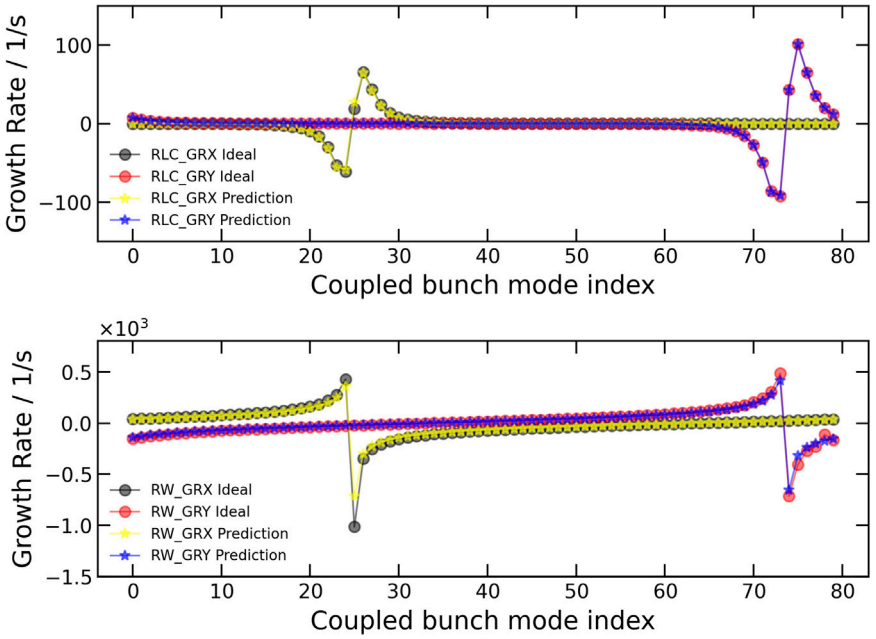

Fig. 9. Growth rate of the transverse coupled bunch modes from RLC (top) and RW (bottom) wakes. The RLC parameters are $R_s = 5.\times10^9\ \Omega/\text{m}^2$, $Q = 1.\times10^3$ and $\omega_r = 2\pi\times4.996\times10^8$ 1/s. The RW parameters are shown in Table 2. The ring is filled uniformly by 80 bunches and each bunch current is 1 mA. The long-range wakes last 20 turns, and the SR damping is turned off. 'Ideal' and 'Prediction' indicate the results are obtained from Eqs. (31) and (32) respectively.

and the excitation time is limited to the first 300 turns. The bunch-by-bunch data of the following 700 turns are used for coupled bunch mode growth rate calculation. The simulation conditions are the same as those used in Fig. 9, except the radiation damping is turned on. The results obtained from Eq. (32) ('Ideal') are also plotted for comparison. Both methods give the same coupled bunch growth rate. Compared to results in Fig. 9, the growth rates are decreased by turning on the radiation damping.

In the longitudinal plane, the tracking studies with the longitudinal long-range wakes can be set up similarly in CETASim.

4.4. Transient beam loading effect

Transient beam loading brings two effects: the longitudinal coupled bunch instability and an unexpected bunch lengthening [26]. In CETASim, the coupled bunch instability can be turned off by ignoring

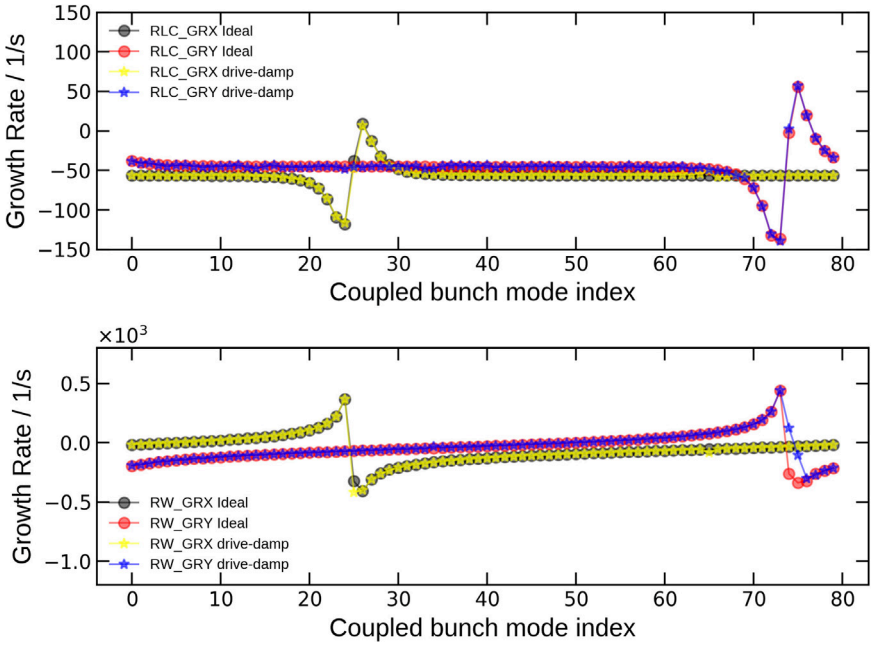

Fig. 10. Growth rate of the transverse coupled bunch modes from RLC (top) and RW (bottom) wakes. The long-range wakes last 20 turns, and the synchrotron radiation damping is turned on. 'Drive-damp' indicates the results are obtained from Eq. (33).

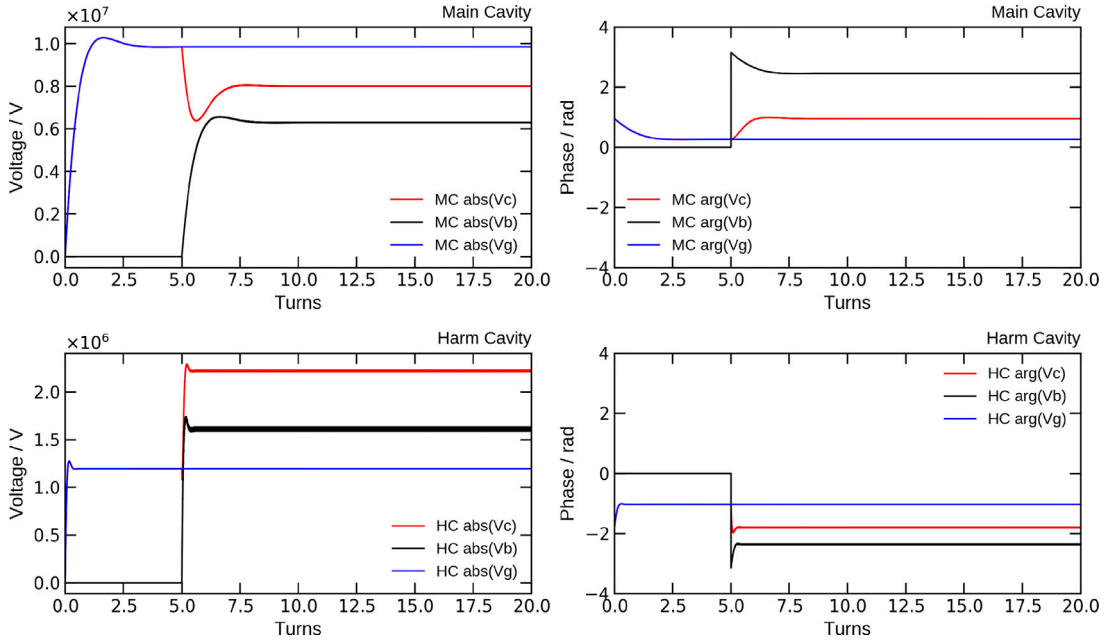

Fig. 11. The amplitude (left) and phase (right) of beam-induced voltage $\tilde{V}_b$, generator voltage $\tilde{V}_g$ and cavity voltage $\tilde{V}_c$ on the main cavity (top) and harmonic cavity (bottom) as function of turns. The beam current is taken into account from the 5th turn.

the dynamical variation of the beam-induced voltage. In that case, the tracking results always converge to an equilibrium state. If tracking is set up as that one bunch is composed of one macro-particle, according to the phase and voltage bunches sampled, the bunch profiles can be found analytically

$$\begin{aligned}\rho(z) &= \rho_0 \exp(-\frac{1}{2\pi h f_0 \alpha_c \delta^2} H_1(z)),\\ H_1(z) &= \frac{h\omega_0^2 e}{2\pi\beta^3 c E}(\Re[\sum_n \int_0^z \tilde{V}_{c,n}(z')dz'] \\ &\quad + \int_0^z \int_{z''}^{\infty} e\rho(z')W_0'(z''-z')dz'dz'').\end{aligned} \tag{34}$$

Here, $H_1(z)$ is the Hamiltonian composed of terms due to the RF potential and the short-range wakes [7], n is the cavity index. If multi-particles are set per bunch, then the bunch profile can be obtained by binning the distribution longitudinally in real space. Table 3 gives the RF parameters of the main cavity and the 3rd harmonic systems in PETRA-IV. The cavities are de-tuned to the 'optimized' condition for the lowest power consumption. The filling pattern of the ring is set as $h = 3840 = 80 \times (20 \times (1+1)+8)$. There exist 80 bunch trains, and in each bunch train, every bucket is occupied by the electron beam except the last 8 buckets. The total beam current is 200 mA. Here, we give the simulation results by turning off the longitudinal coupled bunch instability. Fig. 11 shows how the amplitude and phase of the beam

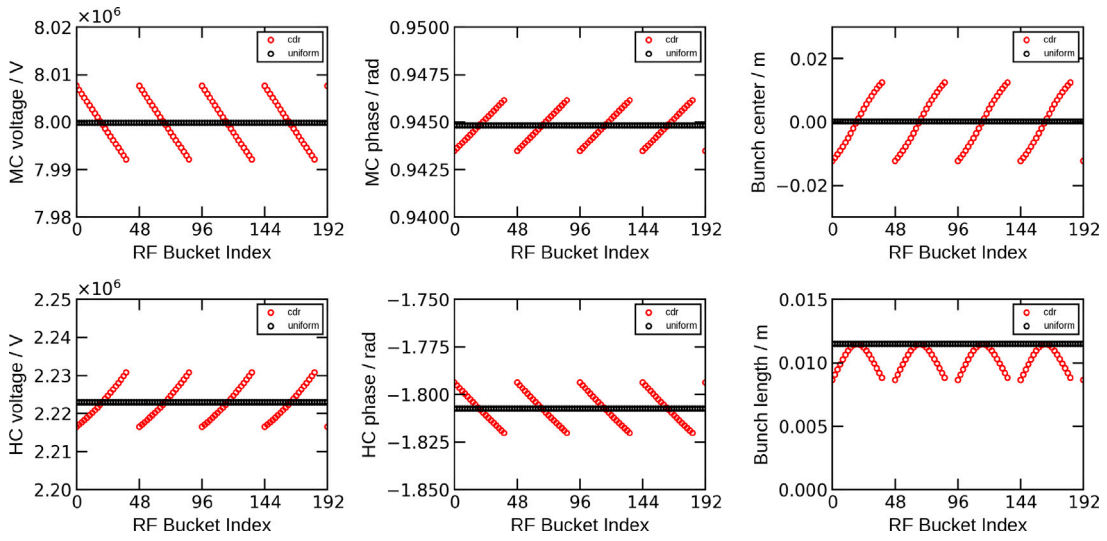

Fig. 12. The cavity voltage $Abs(\tilde{\boldsymbol{V}}_c)$ (left), cavity phase $Arg(\tilde{\boldsymbol{V}}_c)$ (middle) bunch sampled as functions of RF bucket index at the main cavity (top) and harmonic cavity (below); the right column gives the bunch center and bunch length as functions of RF bucket index. The total beam current is 200 mA.

Table 3
RF parameters of PETRA-IV storage ring.

Parameter	Symbol	Main RF ($n = 1$)	Harmonic RF ($n = 3$)
RF freq. (Hz)	$f_{rf,n}$	4.996×10^8	1.499×10^9
Ref. voltage (V)	$V_{c,n}$	8×10^6	2.223×10^6
Synchronous phase (Rad)	ϕ_n	2.516	−0.236
Detuning freq. (Hz)	Δf_n	-27.9×10^3	277.6×10^4
Coupling factor	β_n	3.0	5.3
Shunt impedance	$R_{s,n}$	81.6×10^6	$36. \times 10^6$
Quality factor	$Q_{0,n}$	29 600	17 000
Gen. Curr. Amp. (Amp.)	$Abs(\tilde{\boldsymbol{I}}_g)$	0.626	0.275
Gen. Curr. Phase (Rad)	$Arg(\tilde{\boldsymbol{I}}_g)$	0.947	−1.952
Total generator power (W)	$P_{g,n}$	1.34×10^6	7.40×10^4
Total reflected power (W)	$P_{r,n}$	4.98×10^3	1.09×10^5

induced voltage $\tilde{\boldsymbol{V}}_b$, generator voltage $\tilde{\boldsymbol{V}}_g$ and cavity voltage $\tilde{\boldsymbol{V}}_c$ are built up as functions of turns. The generator voltage driven by $\tilde{\boldsymbol{I}}_g$ is simulated from the $0th$ turn with the optimum de-tuning condition. In contrast, the beam-induced voltage driven by $\tilde{\boldsymbol{I}}_b$ is simulated from the $5th$ turn. The cavity voltage $\tilde{\boldsymbol{V}}_c$ beam supposed to sample converges to the designed values as expected.

Fig. 12 shows the simulation results by setting one macro-particle per bunch. The sub-figures on the left and middle depict the cavity voltage and phase sampled by the bunches in the first 4 bunch trains. The sub-figures on the right show the bunch center shift and length variation. The periodic filling pattern leads to a periodical voltage sampling, further reducing to a periodical bunch center offset and bunch lengthening effect. The bunch profile obtained from Eq. (34) as a function of the RF bucket index is shown in Fig. 13. The result suggests that the bunch lengthening is very sensitive to the phase variation in cavities.

We would like to introduce a simple equation [27], which can be used to estimate the cavity phase modulation $\delta\phi_{max}$ due to the empty gaps δt in a bunch train,

$$\delta\phi_{max,n} = \frac{1}{2}\frac{R_{s,n}}{Q_{0,n}}\frac{2\pi f_{rf,n}}{V_{c,n}} I_{DC}\delta t. \tag{35}$$

With the filling pattern $h = 3840 = 80 \times (20 \times (1 + 1) + 8)$, Eq. (35) gives the peak-to-peak phase variation around 0.0037 and 0.029 rad for the main cavity and harmonic cavity, which are rather good estimation compared to the results from CETASim simulation shown in Fig. 12.

Simulation with macro-particles per bunch can be done similarly. Set 3000 macro-particles in each bunch and turn off the longitudinal

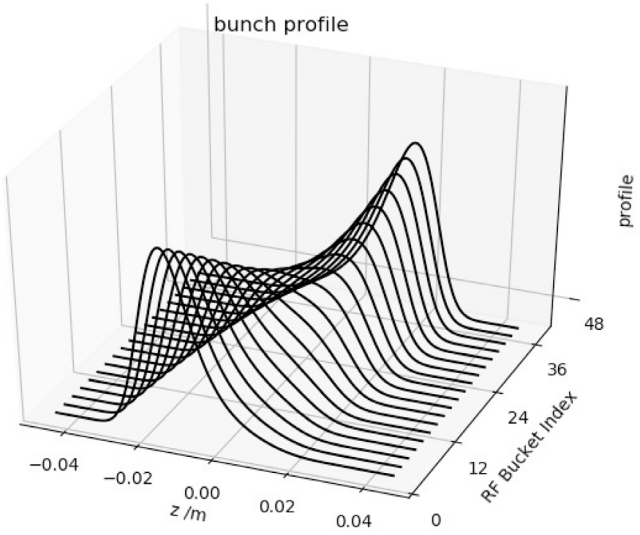

Fig. 13. Bunch profiles in the first bunch train as a function of RF bucket index. The profile are obtained from Eq. (34).

coupled bunch instability in tracking. We give the results of bunch center shift and bunch length variation after 3000 turns in Fig. 14. The bunch profiles are given in Fig. 15. Compared with the results in Figs. 12 and 13, single-particle and multi-particle tracking show good agreements.

The transient beam loading will lead to longitudinal coupled bunch instability once the natural damping is not strong enough. If so, the low-level RF feedback, RF feedforward, or longitudinal bunch-by-bunch feedback have to be applied to stabilize the beam. Here, we briefly introduce the stabilization mechanism when applying low-level RF feedback. Note the cavity impedance as $Z(\omega)$, from the control theory, when the low-level RF feedback is included in the control loop, the impedance sampled by the beam will be modified by

$$Z_{cl}(\omega) = \frac{Z(\omega)}{1 + \exp(-i\omega\tau)G(\omega)Z(\omega)\exp(i\phi)}, \tag{36}$$

where τ is the overall loop delay, ϕ is the loop phase adjusted and $G(\omega)$ is the gain. In Ref. [27], it is shown that the minimum value of

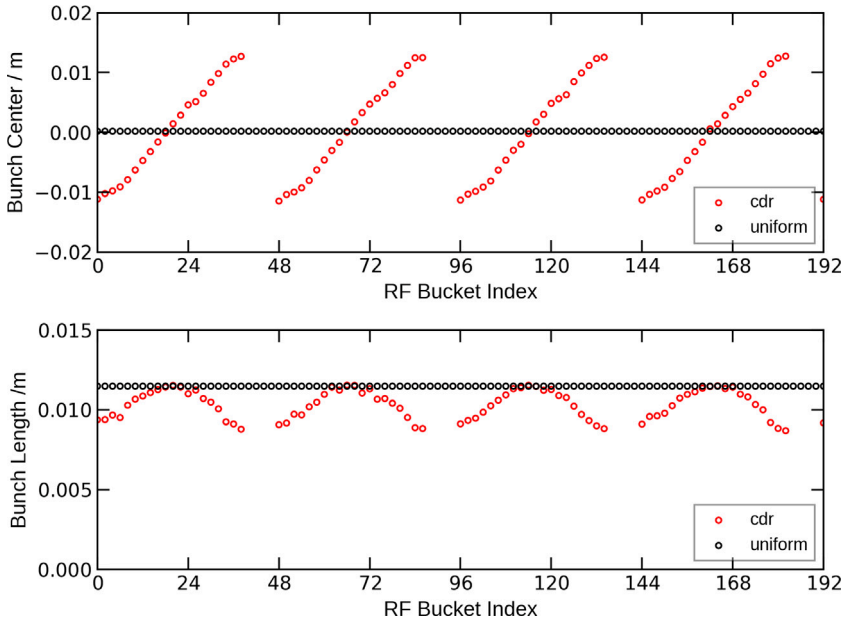

Fig. 14. Bunch center and bunch length variation of the first 4 bunch trains as a function of RF bucket index. The results are obtained from multi-particle tracking, and each bunch is composed of 3000 macro-particles.

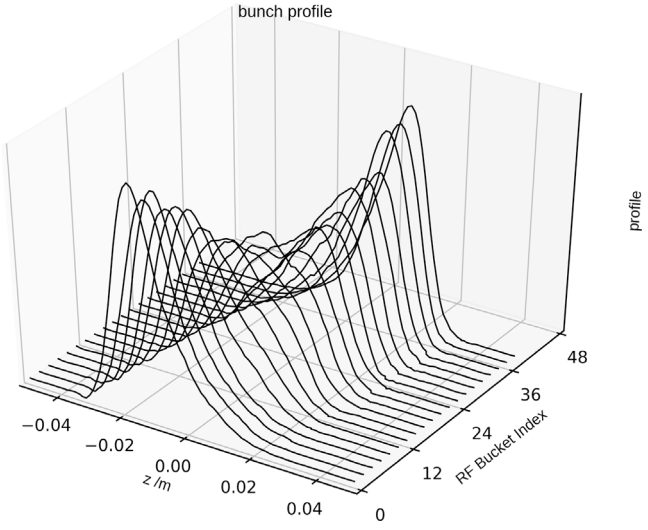

Fig. 15. Bunch profiles as a function of RF bucket index in the first bunch train. The results are obtained from multi-particle tracking, and each bunch is composed of 3000 macro-particles.

the impedance beam can sample is

$$R_{min} = \frac{2}{\pi}\tau\frac{R_s}{Q}\omega_{rf}. \tag{37}$$

For a rough estimation, in the harmonic cavity of PETRA-IV, with an overall loop delay $\tau = 150$ ns, the R_{min} would be decreased by a factor of 20.

In the following, we show the benchmark between CETASim and Elegant of the transient beam loading simulation when the coupled bunch instability is turned on. To stabilize the beam, the shunt impedance of the main cavity and harmonic cavity is reduced by 2 and 20, respectively. Correspondingly, the cavity de-tuning frequencies Δf_n are modified to $\Delta f_1 = -13.953$ kHz and $\Delta f_3 = 13.882$ kHz to maintain the "optimized" de-tuning condition. The beam filling pattern is set as $h = 3840 = 2\times(100\times(1+9)+920)$, which means there are 2 bunch trains, and each train includes 100 bunches. The total beam current is set to 200 mA as well. Fig. 16 compares the beam-induced and generator voltage on the bunch center at the $1000th$ turn. The main cavity and harmonic cavity results from Elegant and CETASim agree well.

4.5. Beam-ion effect

As shown in Eq. (20), ions with a mass number larger than A_c can be trapped in rings. If the oscillation of the trapped ions is confined within the beam pipe, beam-ion instability could be excited. Roughly speaking, with a high bunch charge, ions are over-focused and get lost within the gaps between bunches. With a low bunch charge, more ions can be trapped. However, if the bunch charge is too small, only a few ions can be ionized, leading to a weak beam-ion effect as well [28]. In this sense, we expect the beam-ion effect to be interesting in the medium bunch charge region. In CETASim, the ion motion is limited in the transverse direction. CETASim supplies several parameters to compromise simulation speed and accuracy, such as the number of macro-ions generated per collision, the transverse range beyond which the ions are cleaned, the number of beam-ion interactions per turn, etc. Below, we give two examples of the beam-ion effect simulation in PETRA-IV storage ring, single and multi-ion species. The filling pattern is set as the brightness mode operation scheme, $h = 3840 = 80\times(20\times(1+1)+8)$, and the bunch charges are identical among the 1600 bunches. The total gas pressure is assumed to be 1 $nTor$, and the gas temperature is 300 K. We set one beam-ion interaction point in one turn and take the value of the average betatron function to get the one-turn transfer matrix. In the simulation, one electron bunch is represented by one macro-electron particle. The electron bunch position is initialized on the axis. Ions are cleaned when their transverse distances reference to the ideal orbit are larger than 10 times the maximum effective beam size $abs(\boldsymbol{X_i}) > 10\times(abs(\langle\boldsymbol{x}\rangle) + \boldsymbol{\sigma_x})$.

Set residual gas composed by CO only, Fig. 17 shows the equilibrium transverse ion CO^+ profile in the unit of rms beam size after 10 K turns tracking when the total beam current is 5 mA. For each beam-ion

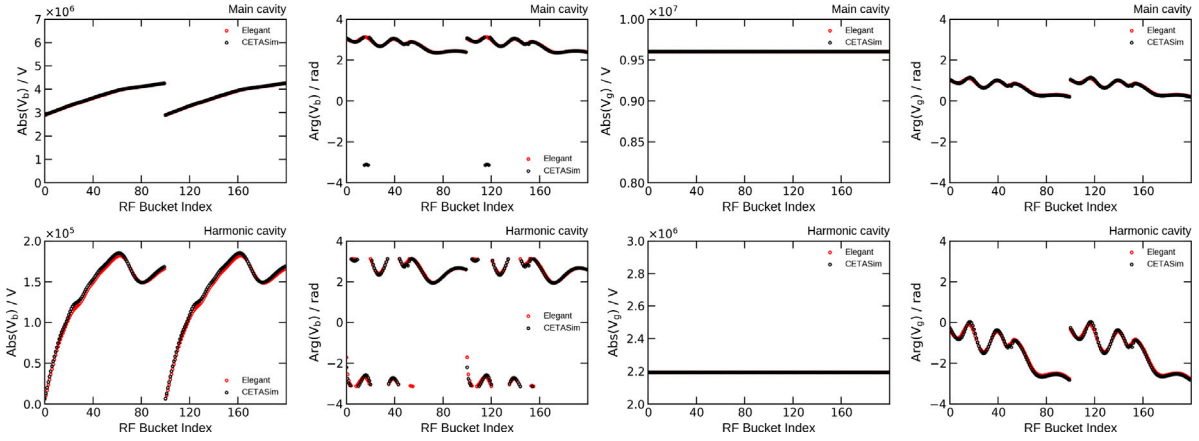

Fig. 16. The amplitude and phase of the beam induced voltage $\hat{V}_b$ and generator voltage $\hat{V}_g$ each bunch sampled at the main cavity (left) and the harmonic cavity (right) after 1000 turn tracking by Elegant and CETASim.

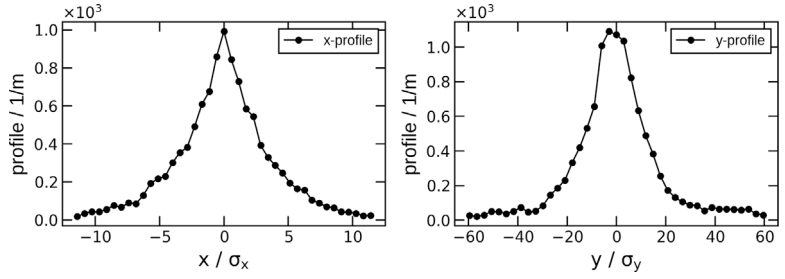

Fig. 17. The equilibrium ionized CO^+ profile on x and y plane in the unit of rms beam size. The total beam current in simulation is set as 5 mA. The profiles of the accumulated ion cloud do not follow the Gaussian shape. The ion gas is composed of CO only.

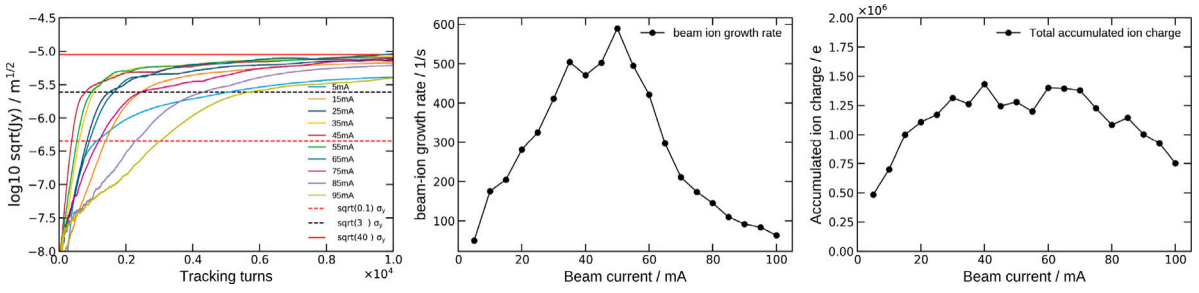

Fig. 18. Left: the square root of the maximum vertical action $\sqrt{J_y}$ among 1600 bunches as a function of tracking turns; Middle: beam ion growth rate as a function of the total beam current; Right: the final accumulated ion charge after 10 K turns tracking as a function of the total beam current. The ion gas is composed of CO only. The maximum bunch action $\sqrt{J_y}$ saturate to a value around $\sqrt{40\epsilon_y}$.

collision, 50 macro-ions are generated. The ion density profile does not follow a Gaussian shape as shown in Ref. [29]. Fig. 18 (left) gives the square root of the maximum vertical action $\sqrt{J_y}$ among 1600 bunches as a function of tracking turns. The action $\sqrt{J_y}$ is defined as

$$J_y = \frac{1}{2}\left(\frac{1+\alpha_y^2}{\beta_y}y^2 + 2\alpha_y y p_y + \beta_y p_y^2\right), \tag{38}$$

where α_y and β_y are the Twiss functions at the beam-ion interaction points. The square root of the bunch action $\sqrt{J_y}$ increases firstly and then gets saturated gradually to around $\sqrt{40\epsilon_y}$. Fig. 18 (middle) gives the growth rate of $\sqrt{J_y}$ as a function of the total beam current. The growth rate is obtained by an exponential fitting of $\sqrt{J_y}$ data selected in between ($\sqrt{0.1\epsilon_y}$, $\sqrt{3\epsilon_y}$), indicating that the beam-ion effect is more severe in the median beam current region. Fig. 18 (right) shows the final accumulated CO^+ charge as a function of the beam current. Again, more ions could be accumulated at the median beam current region.

In the second simulation, the initial gas composition is set the same as that in APS-U [30]. The residual gas comprises H_2, CH_4, CO, and CO_2. The percentage of each gas is 0.43, 0.08, 0.36 and 0.13. Simulation results are shown in Fig. 19. Similar to the results obtained from the single-ion gas setting, the beam-ion effect is more severe in the median beam current region. The $\sqrt{J_y}$ saturates gradually to a value around $\sqrt{20\epsilon_y}$. The growth rate is reduced roughly by a factor of 2. The sub-figure on the right shows the ion charge accumulated after 10 K tuns tracking. Clearly, the higher the total beam current is, the less of the lighter ions can be trapped. The total accumulated ion charge decreased roughly by a factor of 2.

There are several things noticeable in the beam-ion study. Firstly, the beam-ion instability is usually self-limited. Secondly, the growth rate will differ according to the $\sqrt{J_y}$ selected for fitting. Thirdly, the convergence of the simulations as different parameter settings, such as the number of beam-ion interaction points, the number of ions

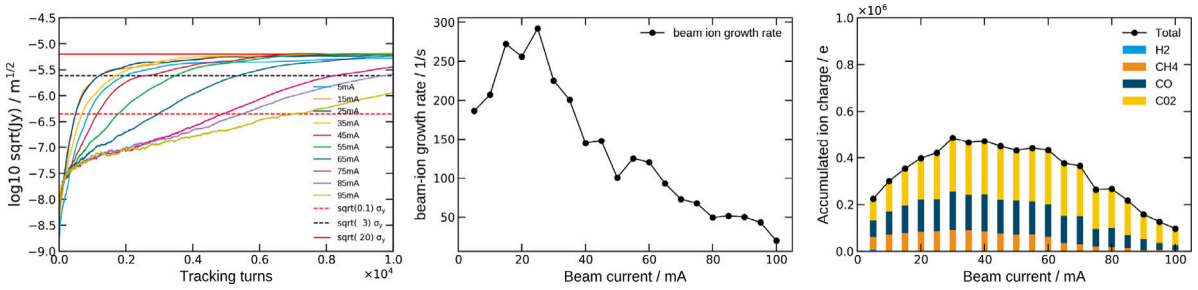

Fig. 19. Left: the square root of the maximum vertical action $\sqrt{J_y}$ among all bunches as a function of tracking turns; Middle: beam ion growth rate; Right: the final accumulated ion charge after 10 K turns tracking. The maximum bunch action $\sqrt{J_y}$ saturate to a value around $\sqrt{20\epsilon_y}$.

generated per beam-ion collision, the range to clean ions, etc, has to be studied beforehand. From our experience, cutting the ring into 10 sections is usually good enough to get the convergence in the ion charge accumulation. Setting 10 macro-ions per collision is a good compromise between simulation speed and accuracy. Set ion cleaning condition m as 10 $(abs(\boldsymbol{X}_i) > m \times (abs(\langle \boldsymbol{x} \rangle) + \sigma_{\boldsymbol{x}}))$ is usually a good choice. The last thing is about the incoherent effect. If one wants to simulate the bunch emittance growth instead of the coherent bunch center oscillation, multi-electron particles can also be set in the simulation. However, in the current version of CETASim, it is still the $Bassetti - Erskine$ model applying to get the Coulomb force among ions and electrons in this "strong–strong" scenario. A Poisson solver based on the Particle-In-Cell methods would be added to the beam-ion module to handle the problem of self-consistence in the 'strong–strong' simulation.

4.6. Bunch-by-bunch feedback

The bunch-by-bunch feedback samples the beam transverse or longitudinal centroid information in the bunch-by-bunch sense [31,32]. Passing these position signals through an FIR filter, the feedback creates bunch-by-bunch momentum kicks to the beam. In Ref. [32], Nakamura shows that the coefficients a_k for an FIR filter can be found by the time domain least square-fitting (TDLSF) method. Here we introduce Nakamura's method for filter design briefly. The oscillation of the beam at the kth turn is approximated by

$$\begin{aligned} x[k] &= \sum_{m=0}^{M} A^m \cos((1+\Delta_k^m)\phi_k^m + \psi^m) \\ &\approx \sum_{m=0}^{M} (P_0^m \cos(\phi_k^m) + P_1^m \phi_k^m \sin(\phi_k^m) + Q_0^m \sin(\phi_k^m) + Q_1^m \phi_k^m \sin(\phi_k^m)) \end{aligned} \tag{39}$$

where M is the number of oscillation of the beam, A^m is the amplitude, ϕ_k^m and $(1+\Delta^m)\phi_k^m$ are the assumed and actual phase advance at the kth turn, P and Q are undefined parameters. In the same way, the output of the filter at the current turn can be found

$$\begin{aligned} y[0] = \sum_{m=0}^{M} & G^m (P_0^m \cos(\varphi^m + \zeta^m) + P_1^m \varphi^m \sin(\varphi^m + \zeta^m) \\ & + Q_0 \sin(\varphi^m + \zeta^m) + Q_1^m \varphi^m \cos(\varphi^m + \zeta^m)) \end{aligned} \tag{40}$$

where G^m and ζ^m are the required gain and phase shift of the FIR filter, φ^m is the assumed phase advance from BPM to the kicker. The FIR coefficients connects $x[k]$ to $y[0]$ with the required values of G^m, ζ^m, φ^m and ϕ_k^m. Assuming the fitting function as $S = \sum_{k=0}^{N} (x[-k] - x_{-k})^2$, the least square fitting method would reduced to the condition

$$\frac{\partial S}{\partial P_i^m} = \frac{\partial S}{\partial Q_i^m} = 0, \tag{41}$$

by which the FIR coefficient a_k can be obtained.

Following this TDLSF method, a preliminary 10-tap FIR filter is designed in the transverse directions for the PETRA-IV storage ring. The FIR filter has a zero amplitude response at the frequency nf_0 (DC rejection) so that the components caused by the closed orbit distortions, unequal bunch signal shapes from pickup electrodes, reflection at cable connections, etc, are filtered out. The information of the current turn is dropped off, indicating a one-turn delay $a_0 = 0$. The first derivative of the phase response curves at the fractional betatron tune νf_0 is designed to be zero to enlarge the phase error tolerance. The normalized amplitude response at the target tune is a local minimum. The filter phase response curve within $(-\pi, 0)$ limits the stable working region. Fig. 20 shows the filter coefficients and the phase and amplitude responses as functions of the tune fractions. In the simulation study, the pickup and kicker are located at the same place, which means the phase responses of the filter at the target tunes have to be $-\pi/2$. If the maximum power P_{max} and the kicker impedance Z_{kicker} are specified in the input file, the kicker voltage will be limited to $\sqrt{2P_{max}Z_{kick}}$.

Fig. 21 compares the transverse coupled bunch mode growth rate due to the RW wakes with and without bunch-by-bunch feedback. The simulation conditions are the same as those in Fig. 9. The 10 taps FIR filter bunch-by-bunch feedback is also applied in tracking. All modes are suppressed. With the same beam condition, we also give the motions of the 80 bunch centroids in the "grow-damped" simulation in Fig. 22. During the tracking, the bunch-by-bunch feedback is turned on from 1000 to 1300 turns and from 1600 to 3000 turns. Without the feedback, the bunches are unstable due to the transverse long-range RW wakes. When the bunch-by-bunch feedback is turned on, oscillations of all of the bunches can be stabilized to zero.

4.7. Emittance exchange and linear coupling

Skew quadrupole leads to a coupling effect between the horizontal and vertical planes, which re-distributes the equilibrium geometrical emittances together with the synchrotron radiation damping and quantum-excitation effects. Here, we note K as the skew quadruple strength with dimension 1/m. In Ref. [33], Lindberg shows a model to predict the equilibrium emittance as a function of the difference of fraction tune Δ_r,

$$\epsilon_x = \epsilon_0 \frac{1 + \frac{1}{4\tau_x}(\tau_y - 3\tau_x)\sin^2\theta}{1 + \frac{1}{4\tau_x\tau_y}(\tau_x - \tau_y)^2 \sin^2\theta} \qquad \epsilon_y = \epsilon_0 \frac{\frac{1}{4\tau_x}(\tau_y + \tau_x)\sin^2\theta}{1 + \frac{1}{4\tau_x\tau_y}(\tau_x - \tau_y)^2 \sin^2\theta} \tag{42}$$

where, $\sin^2\theta = \frac{\kappa^2}{\kappa^2 + \Delta_r^2}$ and $\kappa = \sqrt{\frac{\beta_x\beta_y}{4\pi^2}K^2}$ is the linear coupling coefficient. If the working tune smoothly crosses the difference resonance, the geometrical emittance would be exchanged between the horizontal and vertical planes due to this linear coupling.

An extra skew quadrupole can be set beside the one-turn transfer map Eq. (2) in CETASim to study the effect. The skew quadrupole's strength and the working tunes can be set as ramping variables as a function of the tracking turns. We give two cases for linear coupling studies. The first is the static case in which all the lattice parameters are fixed during tracking. The second one is the dynamical cases, during

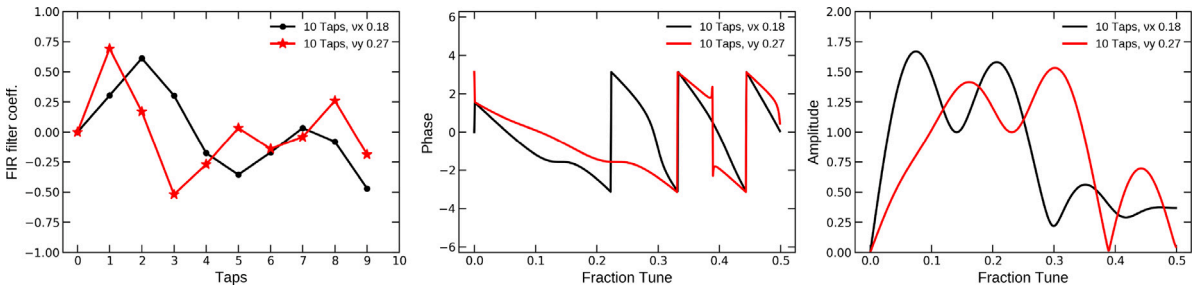

Fig. 20. The horizontal and vertical 10-tap FIR filter coefficients a_k (left), the frequency response of phase (middle) and amplitude (right). The horizontal and vertical target tune fractions are 0.18 and 0.27.

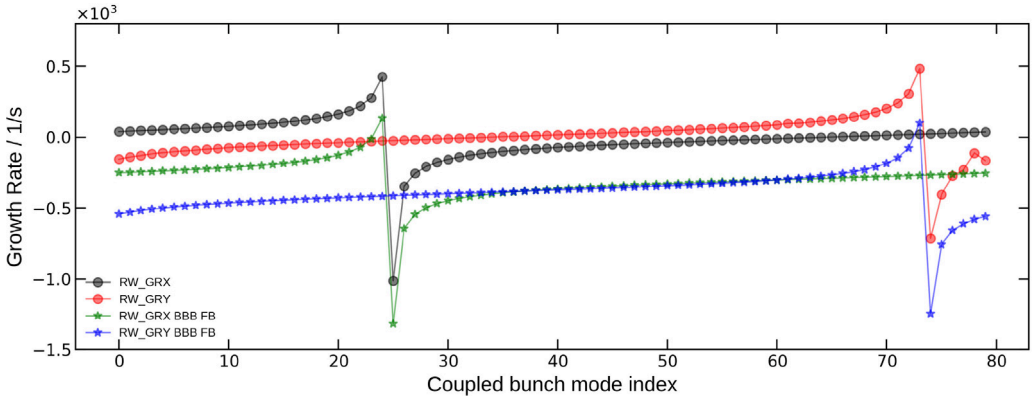

Fig. 21. Comparison of the transverse coupled bunch growth rate due to the RW with and without bunch-by-bunch feedback. The simulation condition is the same as in Fig. 9. The 10 taps bunch-by-bunch feedback shown in Fig. 20 is applied in tracking.

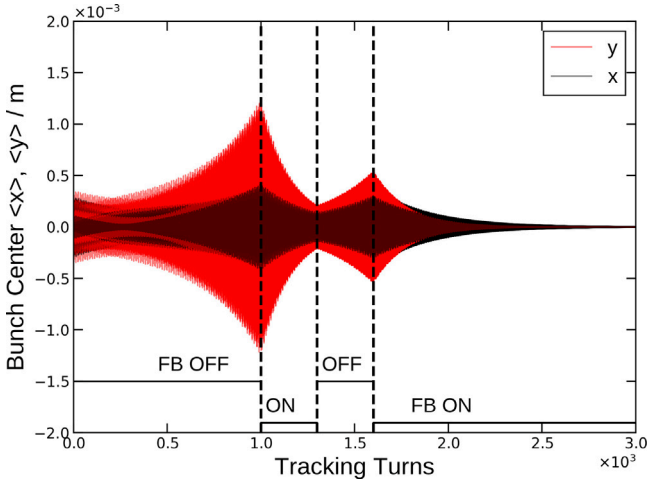

Fig. 22. Trajectories of the 80 bunches centroids. The bunch-by-bunch feedback is turned on from 1000 to 1300 turns and from 1600 to 3000 turns during tracking. The long-range RW wakes are turned on during the whole simulation.

which the difference resonance is crossed by ramping the working tune. Still, the nominal settings of the PETRA-IV lattice and beam condition are applied as the initial conditions. Fig. 23 shows the simulation results from CETASim. The left sub-figure shows the final equilibrium emittance as a function of tune difference in the static simulation. The skew quadrupole strength is set as 0.05 1/m. Tracking results show good agreements compared to the predictions from Eq. (42). The sub-figure on the right shows how the horizontal and vertical emittance are exchanged when the difference resonance is smoothly crossed. The skew quadrupole strength is set to 5×10^{-4} 1/m, and the vertical tune ramps from 0.17 to 0.19 within 10^5 turns.

5. Summary and outlook

The paper introduces the code CETASim, developed recently, in detail. The motivation for CETASim development is to have a simulation tool that covers the collective effects in electron storage rings, especially when different filling pattern schemes are of great concern. The charge of the bunches can be set differently to study the effects of the "guarding bunches", which are normally used for transient beam loading compensation and ion cleaning. The code's architecture is carefully designed to expand the code without too many difficulties if some other beam dynamics have to be considered. Instead of the element-by-element tracking method, CETASim takes the transfer map from sector to sector for simplicity, where the amplitude-dependent tune shift and the momentum compaction factor can be considered up to the second order. Currently, CETASim includes modules to study the single-bunch effects, coupled-bunch effects, transient beam loading, beam-ion effects, and bunch-by-bunch feedback. These modules are benchmarked with results from the theoretical predictions or tracking from Elegant. For the transient beam loading study, the coupled generator dynamics and beam dynamics are treated self-consistently. The coupled-bunch instability can be turned off, which is not physical; however, it can help the user understand how different bunches are lengthened due to different filling patterns.

Still, several things need to be upgraded in the future. The first is to have a subroutine to import the external short-range and long-range wakes and apply them in simulation. As we mentioned in the paper, for the single bunch effect, CETASim takes the impedance as the green function, and for the coupled bunch effect, the long-range wakes are limited to the analytical RW and RCL models. The second one is to have a module to simulate the cavity feedback self-consistently. At this moment, a very simple ideal cavity feedback is available. In the future, we will update the cavity feedback module to cover the real experiment setups with the help of the low-level RF group. The third one is the

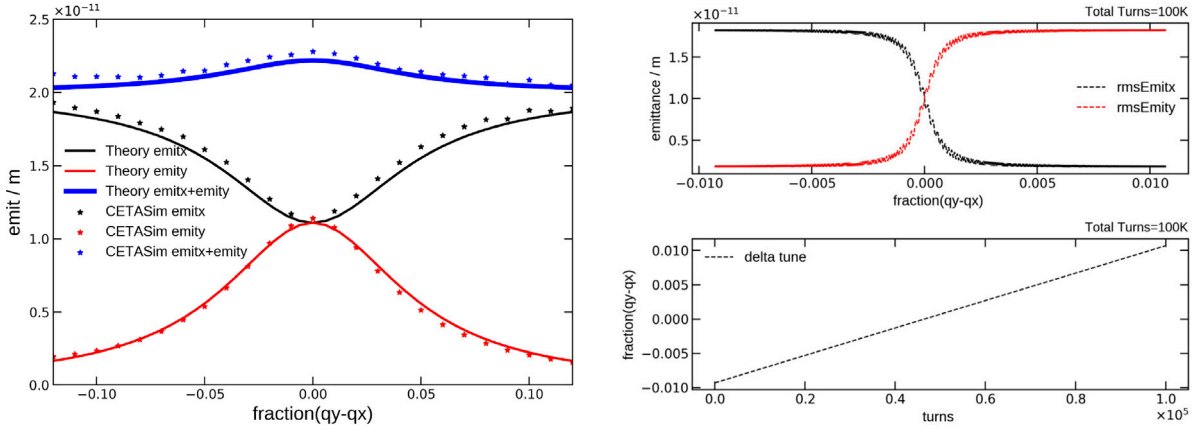

Fig. 23. Left: equilibrium geometrical emittance as a function of distance to difference resonance. Right: The horizontal and vertical geometrical emittance are exchanged when the difference resonance is smoothly crossed in 10^5 turns.

Coulomb interaction between electrons and ions. The $Bassetti-Erskine$ formula based on the 2D Gaussian distribution function is not an accurate approach to get the Coulomb force among the ions and electrons. A self-consistent PIC subroutine will be developed to handle this problem. Finally, we plan to improve the performance of CETASim, including algorithm optimization and parallelization in the future.

CRediT authorship contribution statement

Chao Li: Writing – original draft, Software. **Yong-Chul Chae:** Supervision.

Declaration of competing interest

The authors declare that they have no known competing financial interests or personal relationships that could have appeared to influence the work reported in this paper.

Acknowledgments

The authors thank Dr. Mikhail Zobov from INFN in Frascati for his helpful discussions and Dr. Sergey Antipov for proofreading the manuscript and providing numerous helpful comments and suggestions. This work is supported by the European Union's Horizon 2020 research and innovation programme under grant agreement No. 871072.

Data availability

Data will be made available on request.

References

[1] https://ops.aps.anl.gov/manuals/elegant_latest/elegant.html.
[2] G. Skripka, R. Nagaoka, M. Klein, F. Cullinan, P.F. Tavares, Simultaneous computation of intrabunch and interbunch collective beam motions in storage rings, Nucl. Instrum. Methods Phys. Res. A 806 (2016) 221–230.
[3] https://github.com/PyCOMPLETE/PyHEADTAIL.
[4] https://github.com/ESR-BeamSimulation/CETASIM.
[5] https://ops.aps.anl.gov/manuals/SDDStoolkit/SDDStoolkit.html.
[6] K. Hirata, BBC User's Guide: A Computer Code for Beam-Beam Interactions with a Crossing Angle, Version 3.4, CERN SL-Note-97-57-AP, 1997.
[7] A.W. Chao, Physics of collective beam instabilities in high energy accelerators, 1993.
[8] W. Panofsky, W. Wenzel, Some considerations concerning the transverse deflection of charged particles in radio-frequency fields, Rev. Sci. Instrum. 27 (11) (1956) 967.
[9] S. Vaganian, H. Henke, The panofsky-wenzel theorem and general relations for the wake potential, Part. Accel. 48 (1995) 239–242.
[10] K. Yokoya, Resistive wall impedance of beam pipes of general cross section, Part. Accel. 41 (KEK-Preprint-92-196) (1993) 221–248.
[11] R. Kohaupt, Mechanismus Der Ionenabsangung Im Electron Positron Speicherring Doris, Interner Bericht DESY H1-71/2, 1971.
[12] M. Bassetti, G.A. Erskine, Closed Expression for the Electrical Field of a Two-Dimensional Gaussian Charge, CERN Report, 1980.
[13] To avoid the numerical divergence, in CETASim, Eq. (21) is de-generates to the 1D Gaussian model when $abs((\sigma_x - \sigma_y)/\sigma_y) < 10^{-4}$.
[14] K. Ohmi, Numerical study for the two-beam instability due to ions in electron-storage rings, Phys. Rev. E 55 (1997) 7550–7556.
[15] P. Wilson, Fundamental-Mode Rf Design in E+ E- Storage Ring Factories, Springer, 1994, pp. 293–311.
[16] T. Schilcher, Vector sum control of pulsed accelerating fields in Lorentz force detuned superconducting cavities, 1998.
[17] T. Berenc, M. Borland, R. Lindberg, Modeling rf feedback in elegant for bunch-lengthening studies for the advanced photon source upgrade, in: Proc. of IPAC15, MOPMA006, 2015.
[18] To simulate a passive cavity, the generator current is set as zero.
[19] In the study of transient beam loading effect, the cos convention is adopted, whereas in Eq. (1), it is sin convention.
[20] https://arxiv.org/abs/2408.07995.
[21] https://gitlab.com/IRIS_mirror/IW2D_mirror.
[22] W. Bruns, Gdfidl on massive parallel systems, in: Proc. of Linac, 2002, pp. 416–418.
[23] Y.-C.C. Chao Li, Single Bunch Collective Effect in Petra Iv H6ba Lattice, Report: p4-WP201-rep-0014, 2023.
[24] C. Li, Y.-C. Chae, CETA-a Code Package Being Developed for Collective Effect Analysis and Simulation in Electron Storage Rings, Vol. IPAC2022, JACoW, 2022, WEPOMS033.
[25] G. Rehm, M. Abbott, A. Morgan, New features and measurements using the upgraded transverse multibunch feedback at diamond, in: Proc. IBIC'14, 2014, pp. 696–699.
[26] K.-Y. Ng, Physics of Intensity Dependent Beam Instabilities, World Scientific, 2006.
[27] D. Boussard, Beam loading (particle accelerators), 1995.
[28] C. Li, S. Tian, N. Wang, H. Xu, Beam-ion instability and its mitigation with feedback system, PRAB 23 (7) (2020) 074401.
[29] L. Wang, Y. Cai, T.O. Raubenheimer, H. Fukuma, Suppression of beam-ion instability in electron rings with multibunch train beam fillings, Phys. Rev. ST Accel. Beams 14 (2011) 084401.
[30] https://bib-pubdb1.desy.de/record/426140/files/DESY-PETRAIV-Conceptual-Design-Report.pdf.
[31] M. Lonza, Multi-Bunch Feedback Systems, Cern Accelerator School 2013, 2008.
[32] T. Nakamura, Single-Loop Multi-Dimensional Digital Feedback By FIR Filters, Spring-8, Japan, 2009.
[33] R. Lindberg, Equilibrium Emittances of Coupled Lattices Including Intrabeam Scattering, AOP-TN-2014-020, 2014.